OPTIMIZATION OF COLLAPSED MODE CMUT RECEIVER FOR MAXIMUM OFF-RESONANCE SENSITIVITY

A DISSERTATION SUBMITTED TO

THE GRADUATE SCHOOL OF ENGINEERING AND SCIENCE

OF BILKENT UNIVERSITY

IN PARTIAL FULFILLMENT OF THE REQUIREMENTS FOR

THE DEGREE OF

DOCTOR OF PHILOSOPHY

IN

ELECTRICAL AND ELECTRONICS ENGINEERING

By

Mansoor Khan

July 2018

OPTIMIZATION OF COLLAPSED MODE CMUT RECEIVER FOR MAXIMUM OFF-RESONANCE SENSITIVITY
By Mansoor Khan
July 2018

We certify that we have read this dissertation and that in our opinion it is fully adequate, in scope and in quality, as a dissertation for the degree of Doctor of Philosophy.

Hayrettin Köymen(Advisor)

Abdullah Atalar(Co-Advisor)

Barış Bayram

Yusuf Ziya İder

Ayhan Bozkurt

M. Selim Hanay

Approved for the Graduate School of Engineering and Science:

Ezhan Karaşan
Director of the Graduate School

ABSTRACT

OPTIMIZATION OF COLLAPSED MODE CMUT RECEIVER FOR MAXIMUM OFF-RESONANCE SENSITIVITY

Mansoor Khan
Ph.D. in Electrical and Electronics Engineering
Advisor: Hayrettin Köymen
Co-Advisor: Abdullah Atalar

July 2018

Capacitive Micromachined Ultrasonic Transducer (CMUT) has a flexural conductive plate suspended over a fixed substrate with metal electrode deposited over it. This circular suspended plate is fixed at the rim but is free to move under ambient medium loading or applied bias between CMUT plate and bottom electrode. In presence of an acoustic medium, when the bias is applied the center of the plate deflects more towards the substrate owing to the electric field which is established in the cavity structure. This electric field and ambient force are balanced by plate restoring force in stable region of un-collapsed mode of plate operation. As bias is increased further, the electrostatic forces overwhelms the plate restoring force and the center of the plate contacts with the substrate with a thin insulation layer in between. We call this state, collapse mode of CMUT operation as long as the center of the plate stays in contact with the substrate. In this work, we etch small cavities and employ thin CMUT plate which is easily depressed by the atmospheric force over an evacuated cavity to produce a stable contact with the bottom electrode without any bias.

CMUTs have widely been used as sensors in a wide range of applications such as underwater flow metering sensing, airborne applications, medical ultrasound imaging where CMUTs have been characterized for wide bandwidth and high sensitivity than piezoelectric ceramics. Commercial scanners using 1-D CMUT arrays are also reported to have produced clinical-quality images. Despite the success of CMUTs in medical ultrasound over the past three decades, to this day no effort has been made to optimize the receive sensitivity of a collapsed-mode CMUT.

Traditional practice is to bias the CMUT plate close to collapse voltage to acheive higher coupling coefficent and sense the incoming ultrasound as an open circuit receive voltage (OCRV) signal of the transducer using a voltage pre-amplifier or short circuit receive current (SCRC) employing a transimpedance amplifier. Maintaining plate in the vicinity of collapse threshold is rather difficult as any mechanical disturbance may collapse the plate and compromise the sensitivity of the transducer. In this work we propose ambient pressure collapse CMUT transducer capable of providing a stable performance at off-resonance frequencies. When the plate of a collapsed CMUT is subjected to incoming ultrasound its receive signal becomes a strong function of bias. The electric field sustained between the biased collapsed plate and the substrate is larger than an un-collapsed plate owing to small insulation layer gap at the contact center. This results in an increased input capacitance of collapsed CMUT which together with higher electromechanical turns ratio makes collapsed CMUT a viable choice for a higher acoustic output than its coventional counterpart.

First, we derive and use a linear-equivalent circuit model under small signal conditions to assess the performance of collapsed CMUT as a function of bias. We derive both OCRV and SCRC normalized to incident pressure for a collapsed CMUT in terms of lumped circuit elements. The performance curves as a function of DC bias for varying CMUT operating conditions are obtained. We compare SCRC performance with OCRV and show that simulated SCRC performance with a transimpedance amplifier is not impaired by electrical losses. We then optimize the SCRC performance with bias for any given CMUT operating conditions or geometry.

To characterize the model sensitivity we design and fabricate CMUT cells based on anodic wafer technology. We employ a transimpedance amplifier to measure and verify experimentally through fabricated CMUT cells, -60 dB V/Pa sensitivity at 100 kHz when the CMUT is biased between 50 to 65 Volts.

Keywords: Open Circuit Receive Voltage, Short Circuit Receive Current, Coupling Conditions, Collapse mode CMUT, Off-Resonance Sensitivity, Anodic bonding.

ÖZET

ÇÖKME MODU CMUT ALICISININ REZONANS ALTI DUYARLILIK HASSASİYET ENİYİLEŞTİRİLMESİ

Mansoor Khan
Elektrik ve Elektronik Mühendisliği, Doktora
Tez Danışmanı: Hayrettin Köymen
İkinci Tez Danışmanı: Abdullah Atalar
Temmuz 2018

Kapasitif mikroişlenmiş ultrasonik çevirici (CMUT), üzerine kaplanmış bir metal elektrot ilesabit bir substrat üzerine asılı hareketli iletken bir plakaya sahiptir. Bu dairesel hareketli levhanın kenarları sabittir, ancak ortam yüklemesi veya hareketli plaka ve alt elektrot arasına uygulanan öngerilim etkisi altında hareket etmekte serbesttir. Bir akustik ortamın varlığında ve öngerilim uygulandığında, plakanın merkezi, boşluktaki elektrik alandan dolayı alt tabakaya doğru daha fazla sapmaktadır. Bu elektrik alanı ve ortam kuvveti, çökmemiş plaka çalışma modunun dengeli bölgesinde plaka geriyükleme kuvveti ile dengelenir. Öngerilim voltajı arttıkça, elektrostatik kuvvet, plaka geri yükleme kuvvetini yener ve plakanın merkezi aralarında ince bir yalıtım tabakası kalarak alt metal ile temas eder. Bu, plaka alt tabaka ile temas halinde kaldığı sürece CMUT'un çökme modu olarakadlandırılır. Bu çalışmada, herhangi bir öngerilim olmaksızın, alt elektrot ile kararlı bir temasoluşturmak için içi boş bir oyuk üzerinde atmosferik kuvvetle kolayca basılan ince bir CMUT plakası kullanıyoruz.

CMUT'lar, piezoelektrikseramilere kıyasla bant genişliği ve yüksek hassasiyetle ölçüm yapabilmeleri sebebiyle sualtıakış ölçümleri, uçuş uygulamaları ve medikal ultrason görüntüleme gibi uygulamalarda yaygın olarakkullanılmaktadır.1-D CMUT dizileri kullanan ticari tarayıcıların da klinik yeterlilik kalitesinde görüntülerürettiği de bildirilmektedir. CMUT'lar son otuz yıl içerisinde tıbbi ultrason uygulamalarındaki başarılı kullanımına rağmen, çökmüş modu CMUT'un algılama duyarlılığını optimize etmek için yeterli çaba sarf edilmemiştir.

Genellikle, daha yüksek kuplaj katsayısına ulaşmak ve gelen ultrason sinyalini, voltaj ön yükselteci kullanarak transduser açık devre alıcı voltaj sinyali (OCRV) veya transempedans yükselteci ile kısa devre alıcı akım sinyali (SCRC) olarak

algılamak için CMUT'lara çökme voltajına yakın bir seviyede öngerilim uygulanır. Plakayı çöküş eşiğine yakın tutmak, herhangi bir mekanik parazit plağı çökertebileceği ve dönüştürücü hassasiyetini azaltabileceğinden dolayı oldukça zordur. Buçalışmada, rezonans-altı frekanslarda kararlı bir performans sağlayabilen ortam basıncı çöküşlü CMUT kullanımını öneriyoruz.
Çökmüş bir CMUT plakası gelen ultrasona maruz kaldığında, alınan sinyal öngerilim voltajının fonksiyonu haline gelir. Öngerilme çökmüş plaka ve substrat arasındaki elektrik alan, temas merkezindeki küçük yalıtkan katman boşluğundan dolayı, çökmemiş plakadan dahabüyüktür. Bu çökmüş CMUT'ın, yüksek elektromekanik dönüş oranı ile birlikte giriş kapasitansının artmasını sağlar. Dolaysıyla, yüksek akustik çıkışı sayesinde, çökmüş CMUT'lar muadillerine kıyasla daha uygun bir tercih olmaktadır.

İlk olarak, çökmüş CMUT'ın performansı ve öngerilim sinyali arasındaki bağlantıyı kurmak için, düşük sinyal koşullarında lineer eşdeğer devre modelini türettik ve kullandık. Çökmüş CMUT için, OCRV ve SCRC gelen basınca göre, toplu öğeli devre elemanları cinsinden normalize ettik. Farklı CMUT çalışma koşulları için, DC öngerilimin fonksiyonu olarak performans eğrilerini elde ettik. Simüle edilmiş SCRC performansını OCRV ile karşılaştırdık ve transempedans amplifi katörlü SCRC performansının elektriksel kayıplardan etkilenmediğini gösterdik. Daha sonra, herhangi bir CMUT çalışma koşulu veya geometrisi için SCRC performansını öngerilim ile optimize ettik. Model duyarlılığını karakterize etmek için anodik yonga plakası yapıştırma teknolojisine dayanan CMUT hücrelerini tasardık ve ürettik. Üretilmiş CMUT hücrelerini ölçmek ve deneysel olarak doğrulamak için bir transempedans yükselteç kullanıyoruz. Deneyler 50 – 65 volt arasında öngerilim uygulayarak, 100 kHz frekans değerinde −60 dB V/Pa hassasiyet seviyesinde gerçekleştirilmektedir.

Anahtar sözcükler: Açık Devre Alma Voltajı, Kısa Devre Akımı, Kuplaj Koşulları, Çökme modu CMUT, altı rezonansa hassasiyet, Anodik bonding.

Acknowledgement

Contents

List of Figures

List of Tables

Chapter 1

Introduction

Capacitive Micromachined Ultrasonic Transducer(CMUT), has a suspended conductive plate over a fixed metal electrode lying on a rigid substrate. This suspended plate is clamped at the rims and is free to move under the effect of medium loading or applied bias. When the bias is applied the center of plate deflects towards the substrate owing to the electric field established in the cavity. In presence of an external medium, both the electrical and ambient force are balanced out by the plate restoring force in stable region of un-collapsed mode of plate operation. As the bias is further increased, the electrostatic force may overwhelm the plate restoring restoring force causing the plate to collapse on the substrate. In this work we employ thin silicon plate that is anodically bonded with a pyrex substrate. Thin silicon plate is easliy yeilded by the atmospheric force over an evacuated small gap height making contact with the bottom electrode without any bias. If bias is applied the contact radius of plate increases with the substrate, making it stiffer and less compliant. This effects the sensitivity of collapse mode CMUT as an ultrasound receiver, as plate becomes stiffened due to large bias its receive sensitivity decreases.

In this work we put forth design guidelines in terms of CMUT operating conditions from which the physical dimensions of a collapsed mode CMUT receiver can be derived for maximum sensitivity. Once the operational parameters of collapsed CMUT are set it is then biased in a critical biasing region which produces maximum off-resonance sensitivity.

CMUTs have widely been used as sensors in wide range of applications such as underwater flow metering sensing, airborne applications, in medical ultrasound etc. Over the past three decades CMUTs have made significant progress and has proved to be a viable technology in medical ultrasound owing to its standard silicon integrated circuit (IC) fabrication technology and potential for integration with electronics. For example, the first pulse-echo 128-element, 1-D linear CMUT array was fabricated using simple photolithography process and was characterized for wide bandwidth and high sensitivity than piezoelectric ceramics in 2001 [1]. Commercial scanners using 1-D CMUT arrays are also reported to have produced clinical-quality images [2],[3]. 2-D CMUT arrays with 128 × 128 elements have also been successfully fabricated and characterized [4]. These 2-D arrays can be integrated with electronics in the form of a 3-D multichip module by flip-chip bonding [5]. Recently, tuning of the center frequency of collapsed-mode CMUT is investigated for inter-cardiac echo imaging. In [6] the center frequency of a collapsed CMUT is tuned between 8.7 MHz and 15.3 MHz by varying the DC bias. Maximum transmit sensitivity of 52 kPa/V is achieved at the center frequency of 9 MHz. Despite the success of CMUT technology in broad range of applications in ultrasound imaging, to this day no effort has been made to optimize the receive sensitivity of a collapsed-mode CMUT.

This work demonstrates both analytically and experimentally that a CMUT in collapsed mode of operation could be optimized and used for the detection of ultrasound more efficiently and in a stable manner than that in conventional mode. When the plate of a collapsed CMUT is subjected to ultrasound its receive signal in form of an OCRV or SCRC becomes a strong function of bias. The electric field sustained between the biased collapsed plate and the substrate is larger than an un-collapsed plate owing to small insulation layer gap at the contact center. This reduced gap increases the capacitance, resulting in an improved electromechanical transformer ratio [7],[8]. This makes collapsed-mode CMUT operation a viable choice for higher acoustic output [9] but lower bandwidth than conventional CMUTs [10]. Many studies have developed and used accurate FEM models to show superior power transmission and efficiency in collapsed mode of CMUT operation [11].

In this work, we aim to present performance curves for a collapsed-mode CMUT demonstrating guidelines for CMUT design. We first derive the small signal model for a collapsed-mode CMUT and use this model to derive the SCRC and OCRV performance for varying CMUT operating conditions. We compare SCRC performance with OCRV and show that SCRC is not impaired due to electrical losses. SCRC normalized to incident pressure is then optimized with bias for arbitrary CMUT operational parameters. To characterize the collapsed CMUT performance we fabricate CMUT cells employing anodic wafer bonding technology. The model impedane and predicted SCRC performance is verified experimentally by using a transimpedance amplifier. We measure -60 dB V/Pa amplifier output at 100 kHz over the biasing range of 50 to 65 Volts.

Chapter 2

Linear Circuit Modeling of Collapsed CMUT Receiver

2.1 Analysis of Collapsed CMUT

A cross-sectional view of a collapsed CMUT is shown in Fig. 2.1 where a is the clamped circular plate radius, b is the contact radius, t_g is the gap height, t_i is the insulation layer thickness and t_m is the plate thickness.

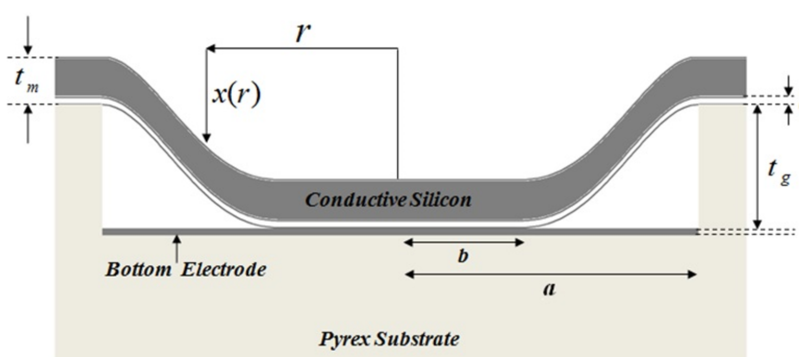

Figure 2.1: Cross-sectional view of a collapsed CMUT cell.

Collapsed CMUT bending profile, $x(r)$, is determined by employing radial dependent electrical force in presence of uniformly distributed mechanical force (due to ambient pressure, P_b) in Timoshenko's formulation of [12],[13].

$$r\frac{d}{dr}\left(\frac{1}{r}\frac{d}{dr}(r\frac{dx(r)}{dr})\right) = \frac{1}{D}\int_b^r \left(P_b + \frac{\epsilon_0 V^2}{2(t_{ge} - x(\zeta))^2}\right)\zeta d\zeta \tag{2.1}$$

where r is the circular plate radial variable, and $D = Y_0 t_m^3/12(1-\sigma^2)$. Y_0 and σ are the Young's modulus and Poisson's ratio of the plate, respectively. The electrical force density is the electrostatic force on the unit area capacitor with the gap, $t_{ge} - x(r)$, having a voltage V across it. $t_{ge} = t_g + t_i/\epsilon_r$ is the effective gap height, and ϵ_r is the relative permittivity of insulation layer.

To avoid a large set of collapse bending profile calculations for each different CMUT design, (2.1) is normalized and rearranged first. We rewrite (2.1) as:

$$\bar{r}\frac{d}{d\bar{r}}\left(\frac{1}{\bar{r}}\frac{d}{d\bar{r}}(\bar{r}\frac{dx(\bar{r})}{d\bar{r}})\right) = 64\int_{\bar{b}}^{\bar{r}} \left(\frac{P_b}{P_g} + \frac{2(V_{DC}/V_r)^2}{9(1 - \bar{x}(\zeta))^2}\right)\zeta d\zeta \tag{2.2}$$

where the normalized variables are:

$$\bar{r} = \frac{r}{a}, \quad \bar{b} = \frac{b}{a}, \quad \bar{x}(.) = \frac{x(.)}{t_{ge}} \tag{2.3}$$

P_g is the pressure required to deflect the plate by its effective gap height, t_{ge} at zero bias and V_r is the bias required to collapse the CMUT plate in vacuum.

$$P_g = \frac{64Dt_{ge}}{a^4}, \quad V_r = \frac{16}{3a^2}\sqrt{\frac{Dt_{ge}^3}{\epsilon_0}} \tag{2.4}$$

(2.2) is solved numerically with the following boundary conditions:

$$\begin{aligned}\bar{x}(\bar{r})\big|_{\bar{r}=1} = 0, \quad \bar{x}(\bar{r})\big|_{\bar{r}=\bar{b}} = \frac{t_g}{t_{ge}}, \quad \frac{d}{d\bar{r}}\bar{x}(\bar{r})\big|_{\bar{r}=1} = 0, \\ \frac{d}{d\bar{r}}\bar{x}(\bar{r})\big|_{\bar{r}=\bar{b}} = 0, \quad \frac{d^2}{d\bar{r}^2}\bar{x}(\bar{r})\big|_{\bar{r}=\bar{b}} = 0\end{aligned} \tag{2.5}$$

For different combinations of CMUT operational parameters P_b/P_g ,V_{DC}/V_r, and t_g/t_{ge} resulting collapsed profile $\bar{x}(\bar{r})$ is calculated numerically in the MATLAB routine described in [14]. In this work, the effect of the profile is given in *rms* plate displacement, X_R defined as follows:

$$X_R = \sqrt{\frac{1}{\pi a^2}\int_0^a 2\pi x^2(r) r dr} \tag{2.6}$$

For the given collapsed CMUT operating conditions the *rms* plate profile of (2.6) is used to define the lumped elements uniquely as polynomials in X_R/t_{ge}. These polynomial expressions for lumped circuit elements are defined in Appendix A. In Fig. 2.2, the variation of normalized bias voltage, V_{DC}/V_r is plotted against normalized plate rms displacement, X_R/t_{ge}, for varying normalized gap heights, t_g/t_{ge} and normalized static pressures, P_b/P_g of 1 and 2.

The curves in Fig. 2.2 are truncated up to 50% plate contact radius with the bottom electrode. If thick insulation layer or a lower normalized gap height like $t_g/t_{ge} = 0.65$ is employed then the biasing required to reach the same plate contact of 50% is 1.4 times the bias required for $t_g/t_{ge} = 0.85$ (thin insulation) at $P_b/P_g = 1$. The static calculations of collapsed plate bending obtained from these curves are then used to define the elements in the lumped model, for applied static bias, V_{DC} and static pressure, P_b.

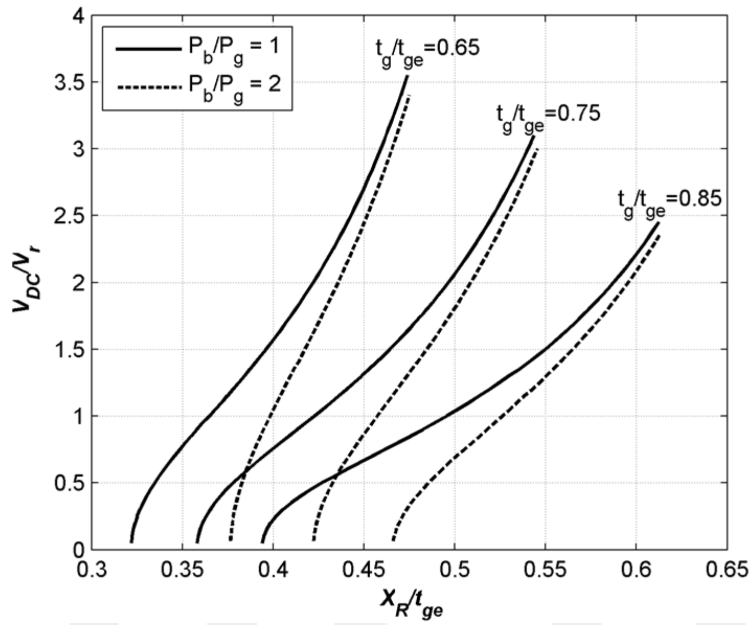

Figure 2.2: Collapsed CMUT plate voltage-displacement interrelation for varying normalized gap heights, t_g/t_{ge} and normalized static pressures, P_b/P_g of 1 and 2.

2.2 Linear Circuit Model for Collapsed CMUT

Collapsed-mode CMUT receiver, under small signal conditions can be represented by a linear equivalent-circuit-model of Fig. 2.4. Small signal circuit parameters are derived by linearizing the transduction and plate restoring force at the static operating point, X_R. Receive CMUT *ac* voltage is V_{ac} at the electrical port and resulting plate displacement is x_r. These *ac* quantities are much smaller than static bias, V_{DC} and plate *DC* displacement, X_R:

$$V^2 = [V_{DC} + V_{ac}]^2 \approx V_{DC}^2 + 2V_{DC}V_{ac} \tag{2.7}$$

$$x_R = X_R + x_r \quad \text{since} \quad |V_{ac}| \ll V_{DC} \quad \text{and} \quad |x_r| \ll X_R \tag{2.8}$$

[0]Capital letters with capital subscripts represent *DC* quantities while small letter with small subscript represent *ac* quantities.

f_R is the electrical transduction force derived from the instantaneous energy, E, due to charge accumulated on the CMUT electrode in presence of electrical terminal voltage, V :

$$f_R = \frac{dE}{dx_R} = \frac{d}{dx_R}\left(\frac{1}{2}CV^2\right) = \frac{C_0 V^2}{2t_{ge}}\, g_c'\left(\frac{x_R}{t_{ge}}\right) \tag{2.9}$$

where C_0 is the clamped CMUT capacitance and $g_c(.)$ is the capacitance polynomial defined in Appendix A. C is the non-linear electrical capacitance given by,

$$C = C_0\, g_c\left(\frac{x_R}{t_{ge}}\right) \tag{2.10}$$

$$C_0 = \epsilon_0 \frac{\pi a^2}{t_{ge}} \tag{2.11}$$

Using (2.7) in (2.9) we linearize the transduction force, f_R around static X_R as:

$$f_R = F_R + f_r = \frac{C_0\left(V_{DC}^2 + 2V_{DC}V_{ac}\right)}{2t_{ge}}\left[g_c'\left(\frac{X_R}{t_{ge}}\right) + \frac{x_r}{t_{ge}} g_c''\left(\frac{X_R}{t_{ge}}\right)\right] \tag{2.12}$$

Ignoring the higher order terms, and the DC force F_R, we write our linear transduction force, f_r in terms of normalized *rms* plate displacement, X_R/t_{ge} as:

$$\begin{aligned} f_r &= \frac{C_0 V_{DC} V_{ac}}{t_{ge}}\, g_c'\left(\frac{X_R}{t_{ge}}\right) + \frac{x_r}{t_{ge}} \frac{C_0 V_{DC}^2}{2t_{ge}}\, g_c''\left(\frac{X_R}{t_{ge}}\right) \\ &= n_R V_{ac} + \frac{x_r}{C_{RS}} \end{aligned} \tag{2.13}$$

where,

$$n_R = \frac{C_0 V_{DC}}{t_{ge}}\, g_c'\left(\frac{X_R}{t_{ge}}\right) \quad \text{and} \quad C_{RS} = \frac{2t_{ge}^2}{C_0 V_{DC}^2 g_c''(\frac{X_R}{t_{ge}})} \tag{2.14}$$

n_R is the electromechanical turns ratio at the static operating point, and C_{RS} is the spring softening capacitance due to applied V_{DC} whose effect opposes the plate restoring force. In terms of normalized quantities (2.14) can be expressed as:

$$n_R^2 = \frac{4}{15}\frac{C_0}{C_{Rm0}}\left[\frac{V_{DC}}{V_r}g_c'\left(\frac{X_R}{t_{ge}}\right)\right]^2 \tag{2.15}$$

$$C_{RS} = C_{Rm0}\left[\frac{2}{15}\frac{V_{DC}^2}{V_r^2}g_c''\left(\frac{X_R}{t_{ge}}\right)\right]^{-1} \tag{2.16}$$

In (2.15) and (2.16) C_{Rm0} is the linear spring compliance in an un-collapsed mode of plate operation:

$$C_{Rm0} = \frac{9(1-\sigma^2)a^2}{80\pi Y_0 t_m^3} \tag{2.17}$$

and V_r is the bias required to collapse CMUT in vacuum (2.4). In collapsed mode, the restoring force has a non-linear dependence on the plate displacement, therefore the restoring force is also linearized around X_R:

$$f_R + F_{Rb} = \frac{x_R}{C_{Rm}(x_R)} \tag{2.18}$$

where $F_{Rb} = (\sqrt{5}/3)\pi a^2 P_b$ is the uniform rms force due to ambient pressure, P_b [15]. Ignoring the higher order terms we can write the linearized compliance at X_R:

$$f_R + F_{Rb} = \frac{X_R}{C_{Rm}(X_R)} + x_r\left[\left.\frac{d(x_R/C_{Rm}(x_R))}{dx_R}\right|_{x_R=X_R}\right] \tag{2.19}$$

$$f_R + F_{Rb} = \frac{X_R}{C_{Rm}(X_R)} + x_r\left(\frac{1}{C_{Rm}(X_R)} - \frac{X_R}{C_{Rm}^2(X_R)}\left.\frac{dC_{Rm}(x_R)}{dx_R}\right|_{x_R=X_R}\right) \tag{2.20}$$

In (2.20) C_{Rm} is defined as a fraction of linear compliance, C_{Rm0}:

$$C_{Rm}\left(\frac{X_R}{t_{ge}}\right) = C_{Rm0}\,h_c\left(\frac{X_R}{t_{ge}}\right) \tag{2.21}$$

We call (2.21) the DC compliance capacitance defined at static operating point X_R/t_{ge} and appears in the second term of (2.20). Third term of Eq.(2.20) is the *ac* plate compliance capacitance which is defined around the static point as:

$$C_{Rm_{ac}}\left(\frac{X_R}{t_{ge}}\right) = -C_{Rm0}\,\frac{h_c^2(\frac{X_R}{t_{ge}})}{\frac{X_R}{t_{ge}}h'_c\frac{X_R}{t_{ge}}} \tag{2.22}$$

$h_c(.)$ is the plate compliance polynomial in X_R/t_{ge}. Coefficients for capacitance and compliance polynomials are tabulated in Appendix A. Series combination of (2.21) and (2.22) yeilds our small signal compliance capacitance, C_{Rms} as:

$$C_{Rms} = C_{Rm0}\left[\frac{h_c^2(\frac{X_R}{t_{ge}})}{h_c(\frac{X_R}{t_{ge}}) - \frac{X_R}{t_{ge}}h'_c\frac{X_R}{t_{ge}}}\right] \tag{2.23}$$

In Fig. 2.3 the normalized series compliance capacitance, C_{Rms}/C_{Rm0} is plotted for varying normalized gap heights, t_g/t_{ge} and static force F_b/F_g of 1 and 2. For $F_b/F_g = 2$ case the plate makes large initial contact with the substrate and therefore is less compliant. As the bias increases, plate stiffens even more with increasing contact making it less compliant with V_{DC}/V_r. The inductance is equal to the mass of plate in *rms* model:

$$L_{Rm} = \pi a^2 t_m \rho \tag{2.24}$$

The small signal model is finally terminated with the collapsed CMUT radiation impedance [16] as:

$$Z_{RR} = \pi a^2 \rho_0 c_0 \{R(ka, kb) + jX(ka, kb)\} \tag{2.25}$$

where $R(ka, kb)$ and $X(ka, kb)$ are the normalized radiation resistance and reactance of collapsed-CMUT transducer and k is the wavenumber, c_o is the speed of sound, ρ_o is the density all specified in the immersion medium.

On the electrical side the small signal capacitance, C_{0dc}, is defined at static X_R/t_{ge} as:

$$C_{0dc} = C_0\, g_c\left(\frac{X_R}{t_{ge}}\right) \tag{2.26}$$

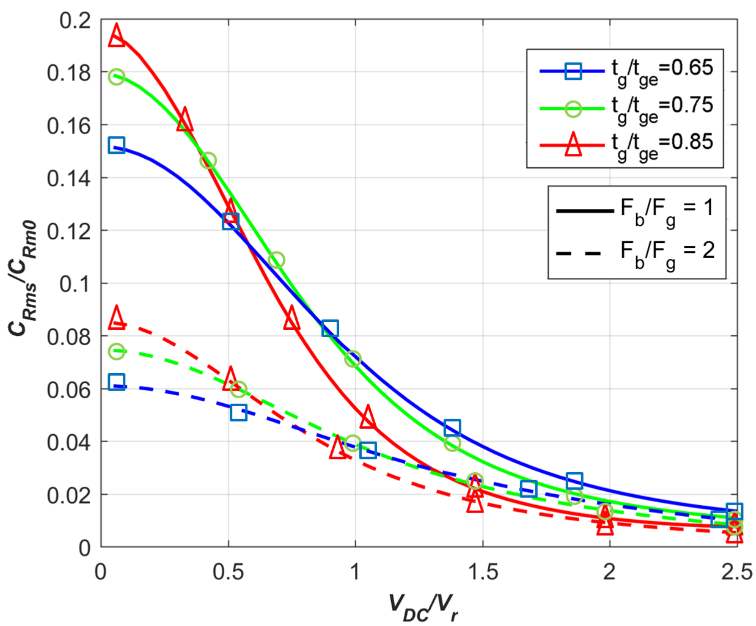

Figure 2.3: Normalized series compliance, C_{Rms}/C_{Rm0} as a function of normalized bias voltage,V_{DC}/V_r for varying normalized gap heights and static pressures F_b/F_g of 1 and 2.

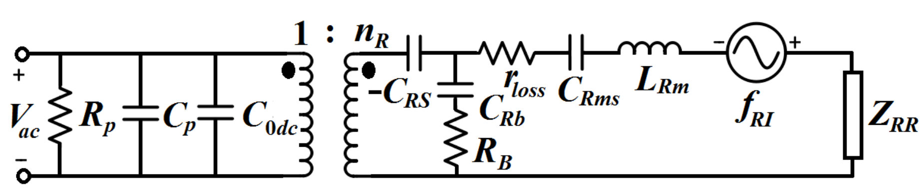

Figure 2.4: Small-signal model of collapsed mode CMUT with dielectric loss and parasitic capacitance.

To complete the electrodynamic behaviour of a a collapsed CMUT transducer. We add external lumped elements to our model to represent both electrical and mechanical losses in the CMUT. On the electrical side C_p is the parasitic capacitance (due to channel connection) and it appears as an additional capacitance in the measured susceptance baseline data. The insulation dielectric loss manifests itself as a baseline at high frequencies in conductance measurements and is modeled by a conductance, G_i:

$$G_i = \omega C_i \tan\delta \tag{2.27}$$

G_i appears parallel with insulation capacitance, C_i. $\tan\delta$ is the insulation dissipation factor. For a typical silicon oxide, $\tan\delta = 0.001$. Eq. (13) of [17] approximates this loss by a parallel resistance, $R_p = 1/(\omega(C_{0dc}+C_p)\tan\delta)$. Both R_p and C_p are additional lumped circuit elements as in [18],[19] and constitute the electrical loss in model.
r_{loss} appears in series with the radiation resistance of the plate and accounts for the internal frictional loss of collapsed plate. It affects both the conductance level and the quality factor of resonance. However, this loss resistance has no effect on the reception performance of the CMUT at off-resonance frequencies.
For a rigid substrate, r_{loss} can be evaluated from the measured and simualted quality factors as:

$$\frac{Q_{simulated}}{Q_{measured}} = \frac{R_{RR} + r_{loss}}{R_{RR}} \tag{2.28}$$

where, $Q_{simulated} = \omega L/R_{RR}$ and $Q_{measured} = \omega L/(R_{RR}+r_{loss})$ are the model and measured qulaity factors of transducer resonance respectively.
(2.28) is only valid for rigid substrate assumption and that when any energy transferred through the gap to substrate is insignificant. For a solid backing, the loss to substrate in the form of spherical waves into the solid half-space or in the form of surface waves in the interfaces is modelled by a parallel impedance branch [20] at the node after $-C_{RS}$ in Fig. 2.4. R_B is the backing loss resistance and is much higher than the plate radiation resistance in air. C_{Rb} is the series compliance of backing material. R_B effects the performance of CMUT and lowers the receive signal SNR as part of the acoustic energy is lost in the backing material. In

presence of R_B, the series loss r_{loss} is lower than what can be obtained from (2.28).

2.3 Electromechanical Coupling Coefficient

The electromechanical coupling coefficient, k_c, of a collapsed-mode CMUT can be derived from its small signal model in terms of circuit parameters. k_c, is defined in the literature [21],[22] commonly as the square root of ratio of converted energy to the total stored energy.

$$k_c = \sqrt{\frac{W_c}{W_{tot}}} \tag{2.29}$$

The total and converted dynamic energies involved in transduction are expressed in terms of our lossless small signal circuit parameters,

$$W_{tot} = \frac{1}{2}V^2\left[C_{0dc} + n_R^2\left(\frac{1}{C_{Rms}} - \frac{1}{C_{RS}}\right)^{-1}\right] \tag{2.30}$$

$$W_c = \frac{1}{2}V^2\left[n_R^2\left(\frac{1}{C_{Rms}} - \frac{1}{C_{RS}}\right)^{-1}\right] \tag{2.31}$$

(2.30) and (2.31) yields the dynamic coupling coefficient as:

$$k_c = \frac{1}{\sqrt{1 + \frac{15 g_c(X_R/t_{ge})}{4\left[\frac{V_{DC}}{V_r} g_c'(\frac{X_R}{t_{ge}})\right]^2}\left[\frac{1}{\overline{C}_{Rms}} - \frac{1}{\overline{C}_{RS}}\right]}} \tag{2.32}$$

where $\overline{C}_{RS}$ and $\overline{C}_{Rms}$ are the *rms* circuit parameters of (2.16) and (2.23) normalized to linear spring compliance C_{Rm0}. The coupling coefficient obtained in (2.32) is plotted with respect to normalized bias voltage, V_{DC}/V_r in Fig. 2.5 for varying normalized gap heights, t_g/t_{ge} and normalized static force, F_b/F_g of 1 and 2. Unlike the conventional mode of CMUT operation where k_c reaches unity irrespective of CMUT operational parameters and value of parasitic capacitance

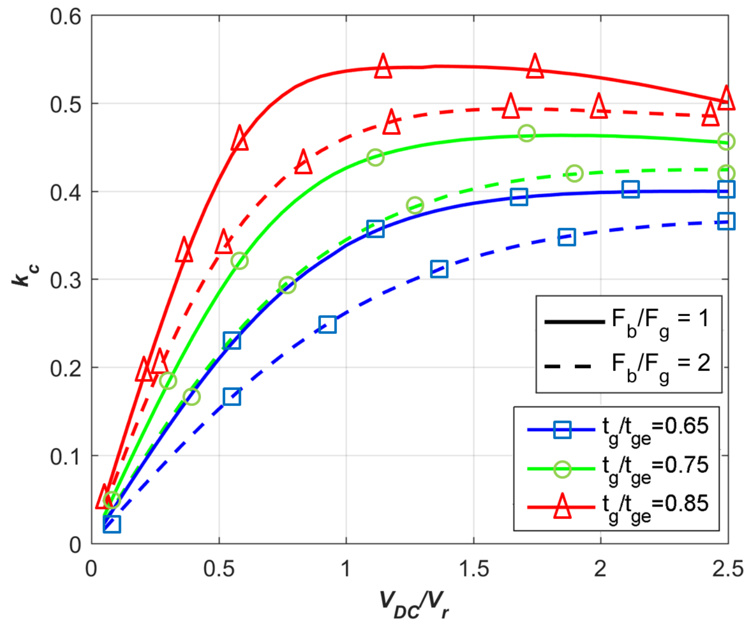

Figure 2.5: Collapsed CMUT coupling coefficient k_c for varying normalized gap heights, t_g/t_{ge} and normalized force, F_b/F_g of 1 and 2; Solid lines for $F_b/F_g = 1$, dashed lines for $F_b/F_g = 2$.

at collapse threshold, collapsed-mode CMUT coupling coefficient is always limited. Therefore, the converted dynamic energy is always limited irrespective of increase in plate contact radius by applying more static bias. Fig. 2.5 demonstrates a higher electromechanical coupling for collapsed CMUTs if a large t_g/t_{ge} is employed, for example when $F_b/F_g = 1$, maximum k_c of 0.54 is achieved at $V_{DC}/V_r = 1$, for t_g/t_{ge} of 0.85.

2.4 Collapsed CMUT Receiver Performance

The performance of a collapsed mode CMUT with silicon plate is derived using entirely normalized expressions. Open circuit receive voltage, V_{OC}, normalized to the incident pressure, p, is expressed in terms of small signal circuit parameters. Channel parasitic capacitance, C_p, normalized to CMUT clamped capacitance,

C_0, is included in the open circuit receive voltage expression to demonstrate its effect on the CMUT reception performance at low frequencies in collapsed mode of operation.

2.4.1 Open Circuit Receive Voltage(OCRV) Sensitivity

OCRV normalized to the product of incident pressure, p, and the cell radius, a, is derived from the small signal equivalent circuit of collapsed CMUT of Fig. 2.4 as:

$$\frac{n_R V_{OC}}{\pi a^2 p} = \frac{\frac{n_R^2}{j\omega(C_{0dc}+C_p)}}{R_R + j\omega(L_{Rm} + X_R) + \frac{1}{j\omega}\left(\frac{n_R^2}{C_{0dc}+C_p} + \frac{1}{C_{Rms}} - \frac{1}{C_{RS}}\right)} \tag{2.33}$$

Both the inductive reactance, $j\omega L_{Rm}$ and the self-radiation impedance, $R_R + j\omega\ X_R$ of a collapsed CMUT cell are small at low frequencies (compared to resonance frequency) and can be ignored in the derivation of off resonance OCRV. Note that (2.33) assumes rigid backing and that any loss to substrate is considered insignificant. Moreover, R_p and r_{loss} does not effect the OCRV at low frequencies and therefore are not included in the derivation. The normalized OCRV then becomes:

$$\frac{V_{OC}}{\pi a^2 p} = \frac{1}{n_R} \frac{1}{1 + \frac{(C_{0dc}+C_p)}{n_R^2}\left(\frac{1}{C_{Rms}} - \frac{1}{C_{RS}}\right)} \tag{2.34}$$

(2.34) can be re-arranged as:

$$\frac{V_{OC}}{p} = \left[\frac{3}{8}\sqrt{\frac{2(1-\sigma^2)}{\epsilon_0 Y_0}}\left(\frac{a^2}{t_m}\right)\sqrt{\frac{t_{ge}}{t_m}}\right] h_1\left(\frac{X_R}{t_{ge}}, \frac{F_b}{F_g}, \frac{t_g}{t_{ge}}, \frac{C_p}{C_0}\right) \tag{2.35}$$

with units of V/Pa. The first term of, V_{oc}/p, gives insight into the dimensional parameters of CMUT for highest receiver voltage sensitivity. It implies that the plate diameter must be as large as possible and it must be thin compared to both the diameter and the effective gap. When expressed in dB, V_{oc}/p becomes:

$$
\left(\frac{V_{OC}}{p}\right)_{dB} = 20log\left(\frac{3}{8}\sqrt{\frac{2(1-\sigma^2)}{\epsilon_0 Y_0}}\right) + 20log(a)
+ 20log\left(\frac{a}{t_m}\sqrt{\frac{t_{ge}}{t_m}}\right) + 20log\left[h_1\left(\frac{X_R}{t_{ge}}, \frac{F_b}{F_g}, \frac{t_g}{t_{ge}}, \frac{C_p}{C_0}\right)\right] \tag{2.36}
$$

For a typical silicon plate:

$$
20log\left(\frac{3}{8}\sqrt{\frac{2(1-\sigma^2)}{\epsilon_0 Y_0}}\right) = -6.8 \text{ dB} \tag{2.37}
$$

The second and third terms of (2.36) depend on the cell dimensions. The last term, $h_1(\frac{X_R}{t_{ge}}, \frac{F_b}{F_g}, \frac{t_g}{t_{ge}}, \frac{C_p}{C_0})$, is a function of normalized parasitic capacitance and CMUT operational parameters, the normalized force, gap height and static normalized *rms* plate displacement:

$$
h_1\left(\frac{X_R}{t_{ge}}, \frac{F_b}{F_g}, \frac{t_g}{t_{ge}}, \frac{C_p}{C_0}\right) = \frac{\sqrt{\frac{3}{2}}\left(\frac{V_{DC}}{V_r}\right)g_c'\left(\frac{X_R}{t_{ge}}\right)}{\left[\frac{V_{DC}}{V_r}g_c'\left(\frac{X_R}{t_{ge}}\right)\right]^2 + \frac{15}{4}\left[\frac{C_p}{C_0} + g_c\left(\frac{X_R}{t_{ge}}\right)\right]\left[\frac{1}{\overline{\overline{C}}_{Rms}} - \frac{1}{\overline{\overline{C}}_{RS}}\right]} \tag{2.38}
$$

h_1 of (2.38) is plotted in Fig. 2.6 for $C_p = 0$ for various normalized gap heights and normalized static force, F_b/F_g of 1 to 2.

2.4.2 Discussion on designing a Collapsed-mode CMUT Receiver for maximum off-resonance OCRV

OCRV multiplier term (plotted in Fig. 2.6) shows that the collapsed CMUT cell must be designed for lowest F_b/F_g and highest possible t_g/t_{ge} with a bias equal to or slightly larger than that required for maximum sensitivity, since the dependence of sensitivity to V_{DC}/V_r is low in maximum region. Increasing the bias thereafter makes the plate less compliant and harder to move implying lower

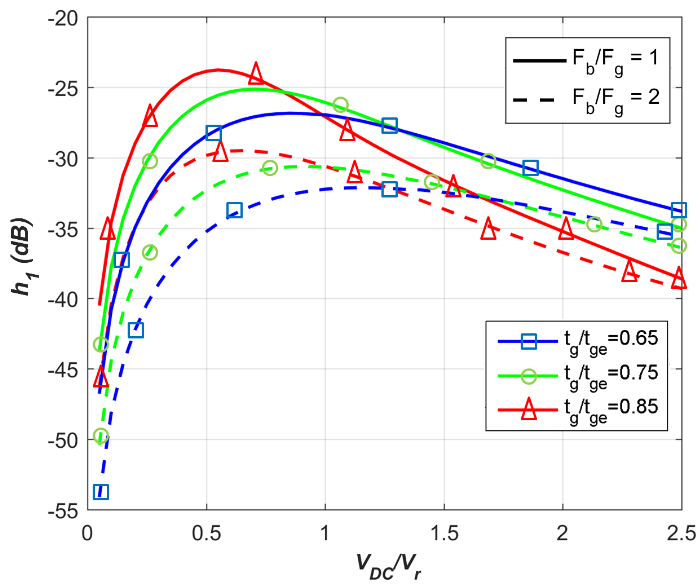

Figure 2.6: Collapsed CMUT sensitivity multiplier term $h_1\left(\frac{X_R}{t_{ge}}, \frac{F_b}{F_g}, \frac{t_g}{t_{ge}}, \frac{C_p}{C_0}\right)$ in dB for $C_p = 0$.

sensitivity. For example, when F_b/F_g is unity, and t_g/t_{ge} is selected 0.85, we obtain -24 dB sensitivity from the multiplier term, h_1, in OCRV transfer function, given V_{DC}/V_r is kept between 0.45 and 0.65.

We observe similar maximum sensitivity regions for higher F_b/F_g, however it is not prudent to choose the dimensions of CMUT for large F_b/F_g, as the plate becomes pre-stiffened due to large static force, resulting in more contact and less sensitivity. Fig. 2.6 shows a loss of 6 dB for the same normalized gap height if the static normalized force, F_b/F_g is doubled. Hence, lower F_b/F_g and maximum t_g/t_{ge} should be employed in receiver CMUT design in collapsed mode for better sensitivity.

Fig. 2.7 demonstrates the effect of relative parasitic capacitance on sensitivity multiplier, h_1, for $F_b/F_g = 1$ and various t_g/t_{ge} values. For a CMUT of similar dimensions that yields $F_b/F_g = 1$ and t_g/t_{ge} of 0.85, 100% parasitic capacitance results in loss of 3 dB. This loss in sensitivity increases for smaller normalized

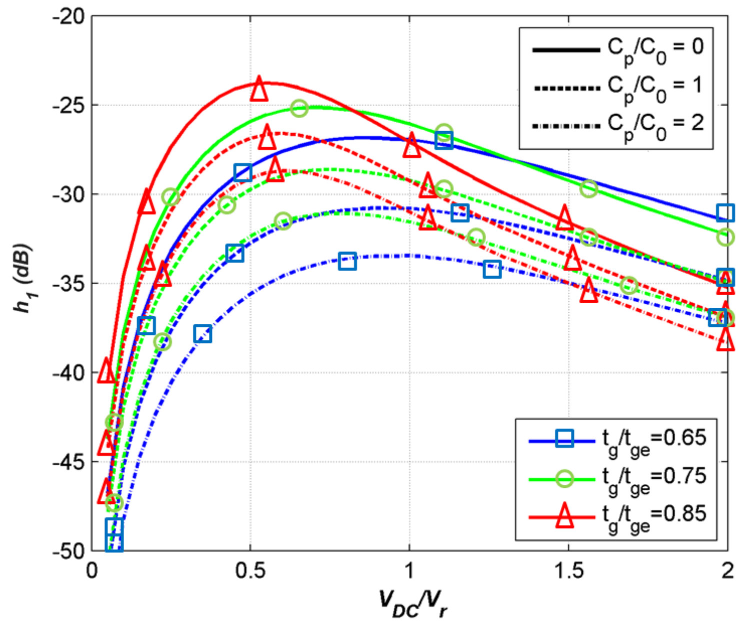

Figure 2.7: Effect of relative parasitic capacitance on collapsed CMUT sensitivity multiplier term, h_1 for various normalized gap heights and $F_b/F_g = 1$.

gap heights for example for normalized gap height of 0.65, the loss is 4 dB for 100% parasitic capacitance in the biasing range of maximum sensitivity region.

2.4.3 Short Circuit Receive Current (SCRC) Sensitivity

SCRC current, i_{SC} (normalized to incident pressure, p) on the electrical side at off-resonance is given by,

$$\frac{i_{sc}}{p} = \pi a^2 \omega n_R \frac{C_{Rms} C_{RS}}{C_{RS} - C_{Rms}} \tag{2.39}$$

For a rigid backing, (2.39) can be rewritten as:

$$\frac{i_{sc}}{p} = \frac{\omega \pi}{5} \left[\sqrt{\frac{\epsilon_0 (1-\sigma^2)}{2Y_0}} \left(\frac{a^4}{t_m} \right) \frac{1}{\sqrt{t_m t_{ge}}} \right] h_2 \left(\frac{X_R}{t_{ge}}, \frac{F_b}{F_g}, \frac{t_g}{t_{ge}} \right) \tag{2.40}$$

with units of A/Pa. The first term contains CMUT geometrical parameters. For high SCRC sensitivity, CMUT must be designed with thin plate and small effective gap height, t_{ge} but with larger aperture radius, a. The second term of (2.40) is given by,

$$h_2\left(\frac{X_R}{t_{ge}}, \frac{F_b}{F_g}, \frac{t_g}{t_{ge}}\right) = \frac{\sqrt{\frac{3}{2}}\left(\frac{V_{DC}}{V_r}\right) g_c'\left(\frac{X_R}{t_{ge}}\right)}{\left[\frac{1}{\overline{C}_{Rms}} - \frac{1}{\overline{C}_{RS}}\right]} \tag{2.41}$$

We can use a transimpedance amplifier to measure SCRC. If we use a capacitance, C_f, as the feedback element, we get a transimpedance gain of $1/(\omega C_f)$, which eliminates ω dependence of (2.40). Note that h_2 is independent of C_p unlike OCRV multiplier term, h_1. Fig. 2.8 plots h_2 for various normalized gap heights and $F_b/F_g = 1$ and 2. h_2 variation with V_{DC}/V_r indicates that a collapsed-mode CMUT has a better SCRC performance than its OCRV counterpart. This is because current on electrical side is scaled by turns ratio, n_R, which increases with the bias and improves the SCRC performance.

2.4.4 Collapsed-mode CMUT Design for Maximum SCRC Performance

We find collapsed CMUT physical dimensions from the operational parameters that maximize, h_2. For example for, $F_b/F_g = 1$ and $t_g/t_{ge} = 0.85$, employing $t_i = 1$ μm thick silicon oxide ($\epsilon_r = 3.9$), with $t_g = 1.45$ μm produces $t_{ge} = 1.7$ μm. A silicon plate with $t_m = 16$ μm and $a = 487$ μm yields $F_b/F_g = 1$. From (2.4) and silicon material properties described in Table I, the vacuum collapse voltage, $V_r = 121.7$ V, that is $V_{DC} = 92$ V is required to obtain $h_2 = -4$ dB. If a transimpedance amplifier is employed with a feedback capacitance, $C_f = 1$ pF then we get a maximum transimpedance amplifier output as -57 dB V/Pa.

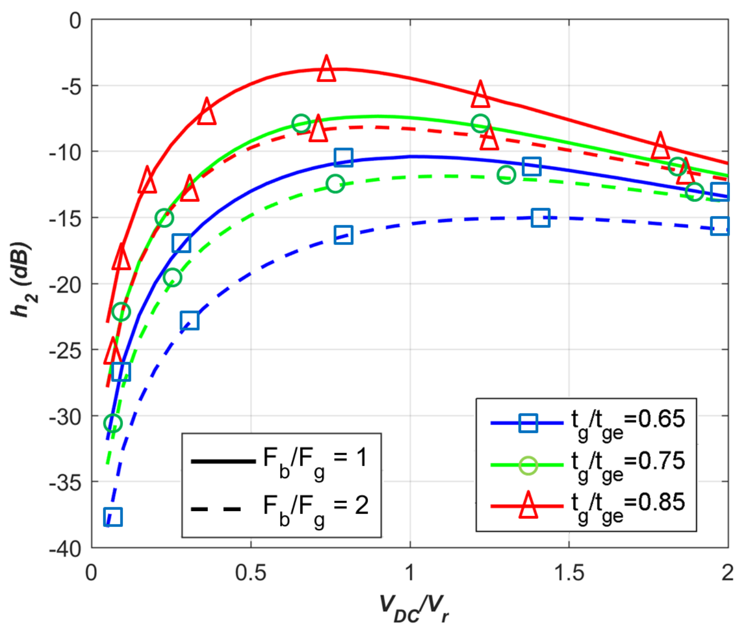

Figure 2.8: Collapsed-mode CMUT SCRC sensitivity multiplier term, h_2 in dB for various normalized gap heights and $F_b/F_g = 1$ and 2.

2.5 Geometric Linearity

2.5.1 Un-collapsed Mode

In [17],[23] the stiffening effect of CMUT plate is modeled, and the operation of CMUT cell in conventional regime was described using a linear mechanical model provided the peak plate deflection to thickness ratio, X_p/t_m remain under 20%, above which the plate is analyzed as a non-linear element in terms of its elasticity. [24] compares the dependency of this deflection-to-thickness ratio, to normalized pressure. The difference observed between the linear and non-linear regions become significant beyond 20% for a varying range of radius-thickness ratio, a/t_m, from 10 to 200. For higher a/t_m ratios this stress stiffening effect cannot be ignored, since in conventional regimes of operation such thin plates are depressed significantly by atmospheric pressure, making the plate stiffer due to induced stress at the rim, although lower quality factors and wide bandwidth have been reported in literature by stiffening the single crystal silicon plate.

2.5.2 Collapsed Mode

Our primary goal in collapsed mode of operation is to find correct static operation point for CMUT plate, which could be otherwise challenging when the X_p/t_m ratio becomes large. Determining the small signal sensitivity will require pre-stressed harmonic response analysis in which geometric nonlinearities are activated during the static analysis to pre-stress the structure. We observed that stiffening effects up-to 50% of peak plate deflection-thickness ratio in collapsed regime are negligible compared to conventional mode of CMUT operation. A similar assessment of this effect is reported in [10], where the comparison of conventional and collapsed-mode CMUT transmit sensitivity is made while keeping the center frequency and bias the same. To maintain the same center frequency at 100 V bias using same plate thickness in both the operating modes of CMUT, the gap height and aperture radius were adjusted so that the plate in collapsed-mode

CMUT has a significantly larger deflection compared to same plate thickness. To model the effect of this large deflection in FEA, a 2-D axis symmetric model of single collapsed CMUT is created in ANSYS[1]. To check the tensile stress of plate in collapsed-mode, both the stress stiffening effects and non-linearity in geometry were enabled in the pre-stress analysis. The effect of the large deflection and the stress stiffening are observed to be negligible for large plate deflections.

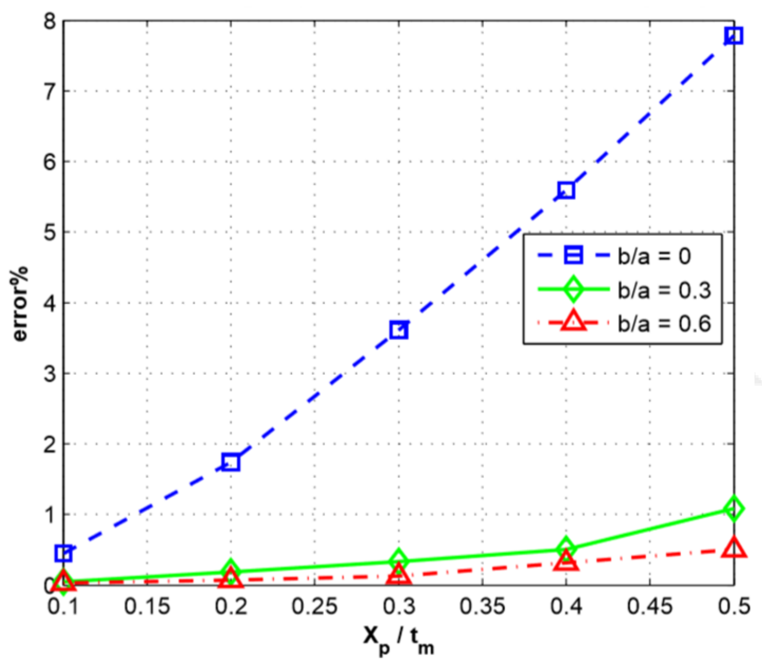

Figure 2.9: Static deflection profile error (taken between obtained plate bending profiles with and without stress stiffening in FEA) versus peak plate displacement to thickness ratio.

In collapsed mode, the plate gets stiffer with increasing contact with the substrate. Due to this pre-stiffening of the plate, the percentage error in the deflection profile is smaller as compared to conventional mode of plate operation. We observe that for normalized contact radius of 30%, the percentage error (with and without stress stiffening) in the plate bending at X_P/t_m of 0.4 is much smaller than the un-collapsed case (blue dashed curve of Fig. 2.8). This error can be further reduced by increasing the plate contact to 60% at the same X_P/t_m of

[1]Static plate bending FEM Simulations are carried out in ANSYS R14.5 (Ansys Inc., Canonsburg, PA). A similar 2-D axis symmetric model of single CMUT is created as in [10].

0.4 (red dashed curve), this decrease in error implies relaxed geometric linearity conditions in collapsed CMUTs for a larger range of X_P/t_m as compared to conventional CMUTs.

In Section 3 the physcial dimensions of fabricated collapsed CMUT cells are such that the peak deflection (etched-gap height, t_g) to plate thickness (t_m) ratio is limited to 0.0625. This small ratio insures that the plate operation remains in linear elastic region.

Chapter 3

Fabrication of Collapsed CMUT Microphone Receiver

We employ anodic wafer bonding technology similar to one desribed in [25] to produce collapsed CMUTs. A design flowchart showing involved fabrication processes is depicted in Fig. 3.1.

A (100) orientation, p-type, boron doped, SOI wafer having 1-μm top layer thermal oxide on 15-μm thick device layer[2] is used as a CMUT plate and a (4-inch wide, 3.3 mm-thick) Pyrex wafer is used as the substrate. The SOI wafer has 1-μm-thick buried oxide (BOX) layer between the device layer and 350-μm thick silicon handle layer. Figure 3.2 shows cross-sectional FIB/SEM photograph of a SOI wafer used in this process. The cross-sectional SEM measurement shows ± 1 μm variation in plate thickness, t_m. This deviation in the overall plate thickness (of Table 4.1) shifts the measured resonance of CMUT plate to lower frequencies as shown in the admittance measurments of Section 4.1

[2]Device Si layer has a 0.01-100 Ωcm resistivity range.

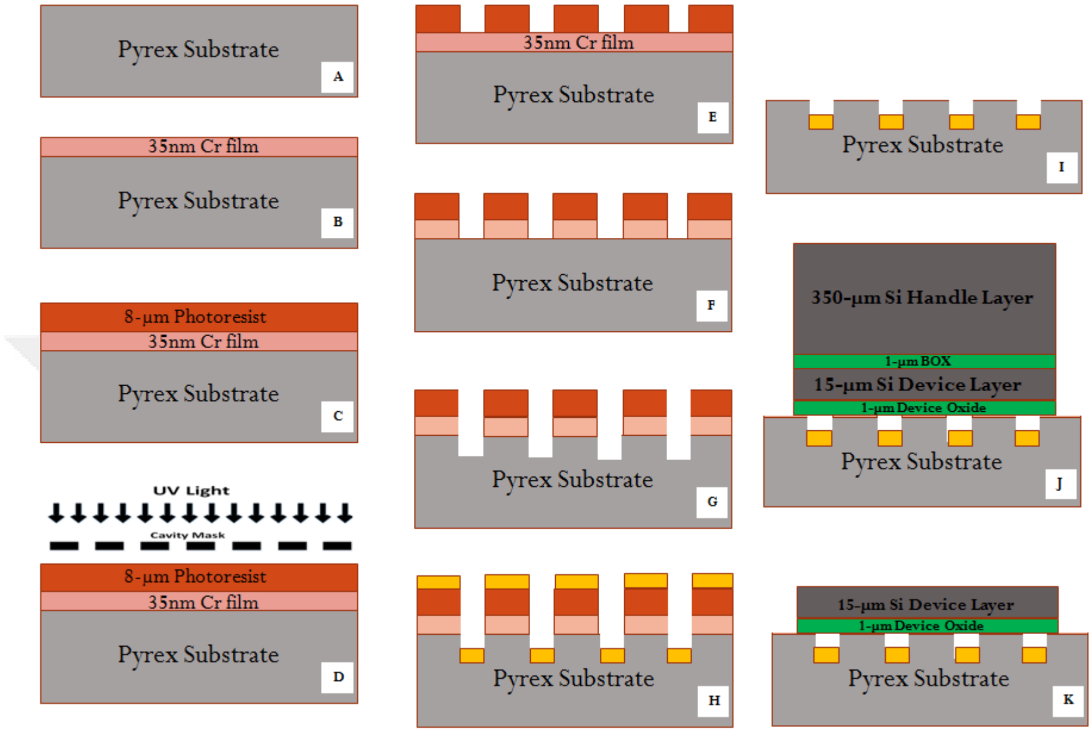

Figure 3.1: CMUTs fabrication flow performed at UNAM Bilkent University using surface micromachining technology.

3.1 Photolithography Process

Following the standard Pyrex wafer clean process[2], the glass substrate is heated at 110°C for 30 mins on a hot plate and is then prepared for chrome deposition before lithography process. 35-nm of Cr is first deposited on the Pyrex wafer in an e-beam evaporation chamber, followed by 8-μm thick spin coat of AZ4562 photoresist of Microchemicals[3]. The resist film is then exposed to 100 mJ of UV under a CMUT feature chrome mask. UV exposed resist film is then developed in a (AZ400k 1:4 DI water) developer solution for about 10 minutes to reveal CMUT features. Fig. 3.4(a) shows Pyrex after lithography with CMUT device features. Developed resist film is then hard baked at 120°C for 1.5 hours and at 150°C for another 1.5 hours on a hot plate. Hard baking of resist film is recommended to

[2] Acetone Sonication/IPA/DI water/Nitrogen blow
[3] Microchemicals GmbH, Ulm, Germany

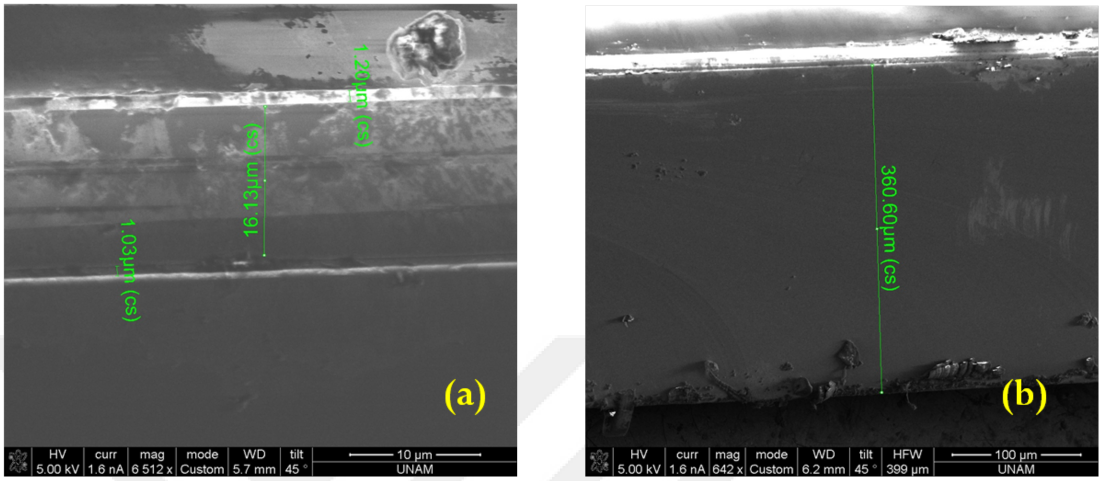

Figure 3.2: (a) Cross-sectional - FIB/SEM of CMUT plate (b) Silicon handle layer thickness.

avoid any peeling or breakage of reisist film owing to long exposure of resist to wet-etch.

Before etching CMUT cavities on pyrex, exposed Cr is removed by a Cr wet etch remover. For this purpose the wafer is left in the chrome remover solution for 2 mins. The addition of thin chrome film underneath the resist helps in avoiding any undesirable anisotropic undercuts.

3.2 Wet-Etch and Metallization Process

After chrome removal, Pyrex wafer was left in a wet-etch (BOE 7:1) bath for 50-mins at room temperature. This produced circular CMUT cavities having a gap height of 1.12-μm. CMUT cavities and electrical pads are connected by a 50-μm-wide channel. 100-nm-thick titanium adhesion layer is first e-beam evaporated and deposited in etched CMUT cavities and channels. After the titanium deposition, 30-nm thick platinum buffer layer is deposited followed by 50-nm of gold layer deposition. For the removal of excess metal on top of photoresist, it was lifted-off by immersing the wafer in piranha solution for 2 mins. Fig. 3.4 (b) and Fig. 3.4 (c) shows the Pyrex wafer after metallization and lift-off.

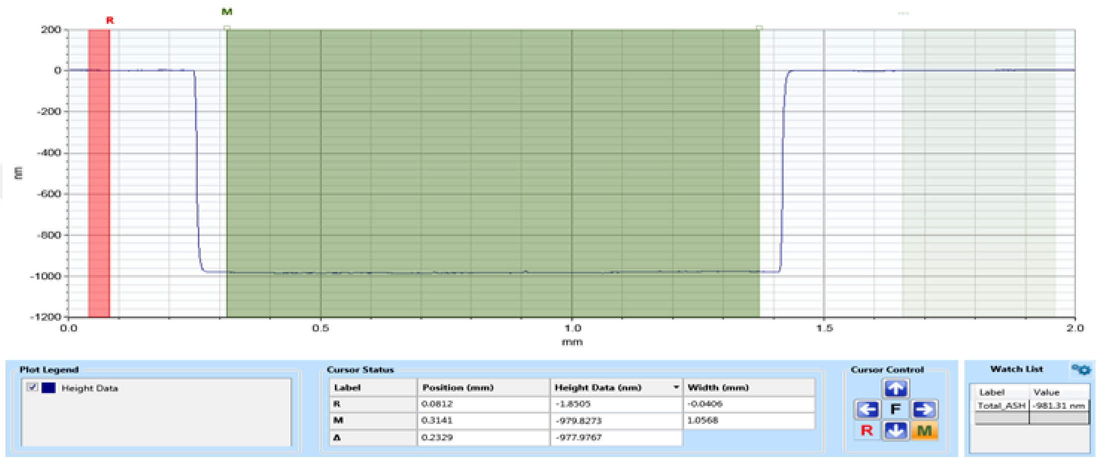

Figure 3.3: Gap height of CMUT features, t_g of about 1 μm is measured by Stylus profilometer after metallization and before bonding. All CMUT features on pyrex have the same gap height.

3.3 Anodic Bonding and Si handle removal process

For the exposure of connection pads on 4-inch Pyrex, 4-inch round SOI is diced into a 2.55-inch octagon and is then anodically bonded with Pyrex from the device oxide side of the silicon device layer. In the anodic wafer bonding process the SOI is bonded to pyrex using specific pressure, electric field and temperature. Pyrex has mobile ions at the bonding temperature in order to maintain the migration of ions and formation of a depletion layer at the interface. The processed Pyrex wafer containing CMUT features were bonded with an octagonal diced SOI at a commercially available bonding facility[4]. After bonding, the interface of the air gaps between SOI and glass substrate, are sealed with a low-viscosity epoxy

[4]Applied Microengineering Ltd., Oxfordshire, UK

resin[5]. Epoxy resin is first mixed with the hardener in ratio (3:1) by weight and is then applied on the rim of the bonded SOI to seal the channel air gaps at the interface of Pyrex and silicon. The wafer is then left in a vacuum chamber at room temperature for 16 hours. This ensures that the gas in the CMUT cavities is sucked out through epoxy. Epoxy is then is cured in an oven at 120° C for 5 hours.

To reveal the collapsed CMUT profiles and for subsequent electrical connections, first 350-μm thick silicon handle layer is removed by SF_6 based RIE process run inside an ICP chamber. To protect the exposed gold pads on pyrex from SF_6 plasma, a 4-inch donut shaped aluminum ring is used as an etch mask. The BOX acts like an etch stop layer for this process, which is then removed by BOE 7:1 to reveal device silicon layer. (Fig. 3.4(e) and Fig. 3.4(f))

3.4 Electrical Connections

The electrical connections on the device silicon and pads are made through a conducting silver epoxy. For device silicon connection, the native silicon oxide is first removed by BOE 7:1. Device wire connection through silver epoxy is applied immediately after the oxide removal. The electrical connections to the bottom CMUT electrodes are achieved using contact pads. The size of these exposed gold pads shown in Fig.3.4 (d) is 3×3 mm. The exposed gold pads are also given wire connections through the same conducting silver epoxy. After putting wires, the epoxy is cured at 67°C for 4 hours.

[5]Biresin CR122 epoxy resin and CH122-3 hardener, Sika, Baar, Switzerland.

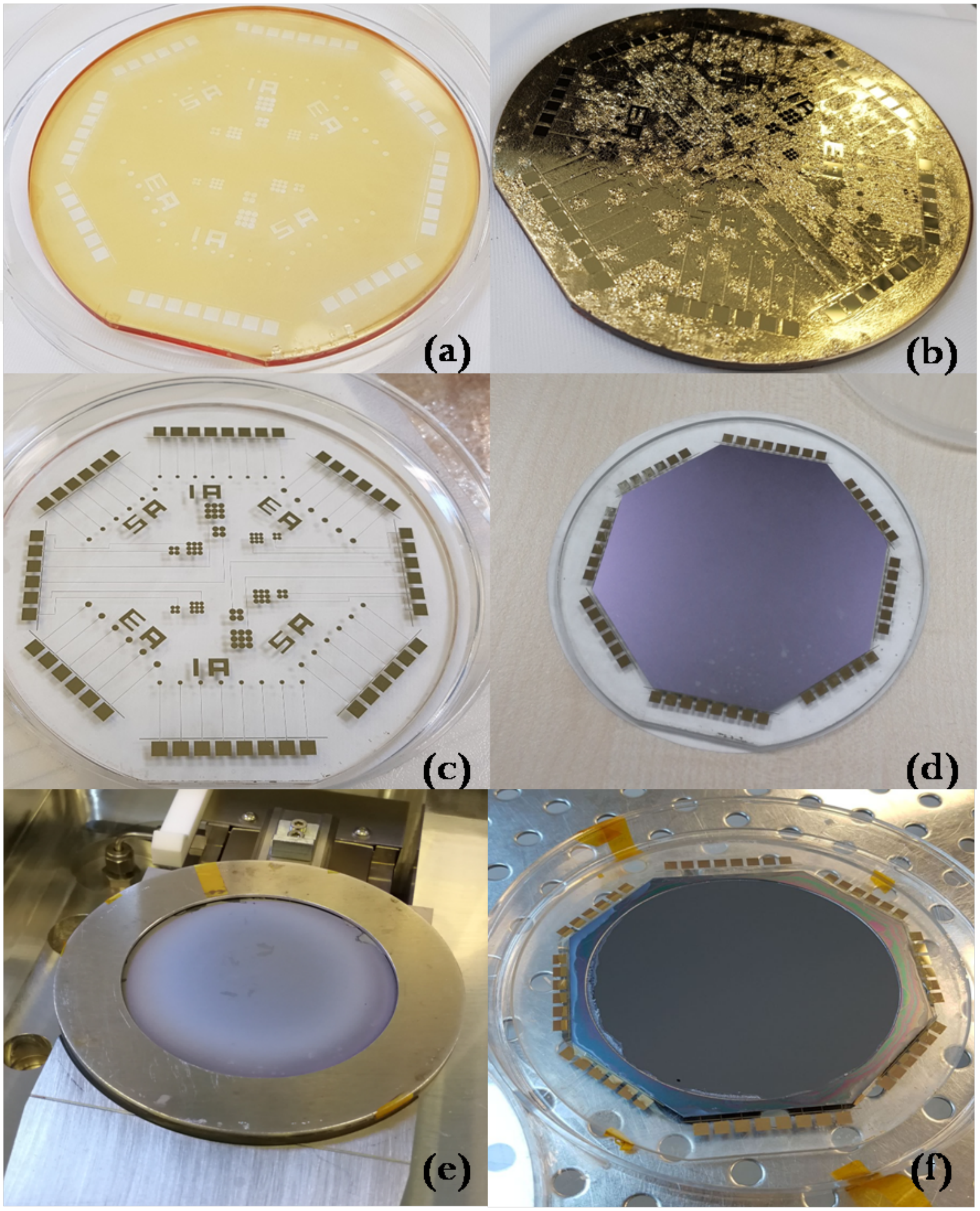

Figure 3.4: (a) Developed CMUT features on a hard baked resist film after chrome removal (b) Post wet-etch and metallization of Pyrex wafer (c) CMUT bottom electrode patterning after lift-off (d) Anodic bonding of diced SOI and processed pyrex wafer (e) Alumunium ring used to cover gold pads in RIE process (f) Silicon device layer after BOX removal.

Chapter 4

Measurements and Model Characterization

We characterize the small signal model experimentally by making collapsed CMUT cell measurements in air. First, the electrical input admittance is measured. From the obtained conductance measurements, we observe and record fabricated collapsed CMUT cells resonance frequency, its quality and losses (both electrical and mechanical). Effective model capacitance is obtained from the susceptance baseline measurements, additional parasitic capacitance, C_p, is then added to the model that constitutes electrical loss along with the dielectric loss resistance, R_p. Performance of collapsed CMUT cells at low frequencies is measured by transmitting a 1 ms tone burst signal and measuring the amplitudes of receive CMUT envelopes on an oscilloscope (See Fig. 4.3). Off-resonance CMUT performance is then compared with model predictions for varying static bias.
To validate the model predictions against measurements we used two fabricated CMUT designs, CMUT-I and CMUT-II, parameters of which are given in Table 4.1. Optical photographs of both fabricated CMUT cells taken from the rear Pyrex side is shown in Fig. 4.1.

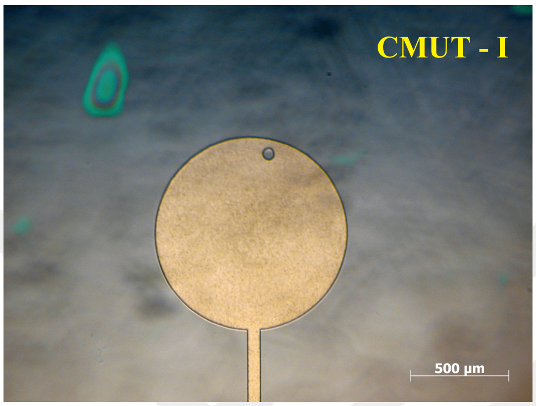

(a) CMUT-I

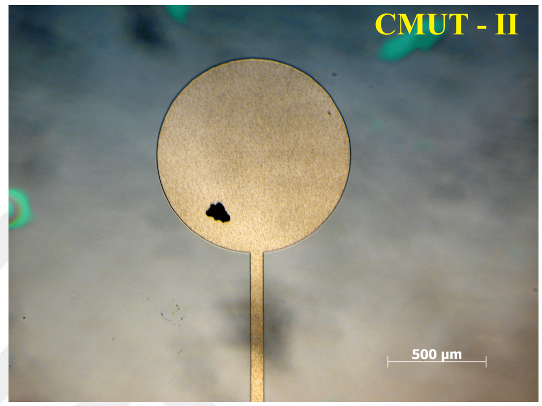

(b) CMUT-II

Figure 4.1: Optical photos of CMUT bottom electrodes taken from the rear Pyrex side after bonding.

Table 4.1: Dimensional Parameters of two fabricated CMUT cells

		CMUT-I	CMUT-II
a	Plate radius (μm)	487.6	489.7
t_m	Plate thickness (μm)	16	16
t_{ge}	Effective gap height (μm)	1.2	1.19
t_i	Insulation layer (μm)	1	1
F_b/F_g	Normalized static force	1.29 @ 0.9 bar	1.33 @ 0.9 bar
t_g/t_{ge}	Nomalized gap height	0.79	0.78
Y_0	Young's Modulus (GPa)	148	148
ρ_m	Si plate density (kg/m^3)	2370	2370
σ	Poisson's ratio	0.17	0.17
ϵ_r	Dielectric Constant	3.9	3.9

4.1 Admittance Measurements

The small signal model of collapsed CMUTs is experimentally validated by first measuring the admittance of fabricated cells in air with an impedance analyzer (HP 4194A). The admittance measurements are made in long averaging mode with 20 V of bias voltage and 0.5 V_{pp} of AC voltage. Measured conductance of both collapsed cells, CMUT-I and CMUT-II are shown in Fig. 4.3. As seen in Fig. 4.3 measured fundamental resonance of fabricated cells is at 650 kHz, with the quality factor of 68.

Small peaks observed at frequencies higher than the main resonance in the impedance measurements are the lowest plate asymmetrical modes of the collapsed CMUT after the first symmetrical mode at 645 kHz and below the second symmetrical mode at 1.8 MHz. Collapsed CMUT plate symmetrical and asymmetrical modes are extracted from the modal analysis in FEM simulations and are shown in Fig 4.2. Asymmetrical modes of the plate are excited due to small asymmetries arising from production inaccuracies. Table 4.2 lists the collapsed plate modes and their frequencies.

The radiation resistance of spherical waves propagating in isotropic solids is derived by Blake in [26]. Baseline of the measured conductance is reproduced by R_B which is 10 times larger than plate radiation resistance for CMUT-I in air with a series loss of $5.6S\rho_0c_0$. For CMUT-II, R_B is 3 times plate radiation resistance with a series loss of $4.5S\rho_0c_0$. This series loss (due to friction of collapsed plate) together with the backing loss, lowers the overall SNR of the received signal. We observe that this series loss is significant in collapsed mode of CMUT operation compared to other losses such as energy coupled to the surface or to the substrate bulk at the rim in un-collapsed mode of CMUT operation in [17].

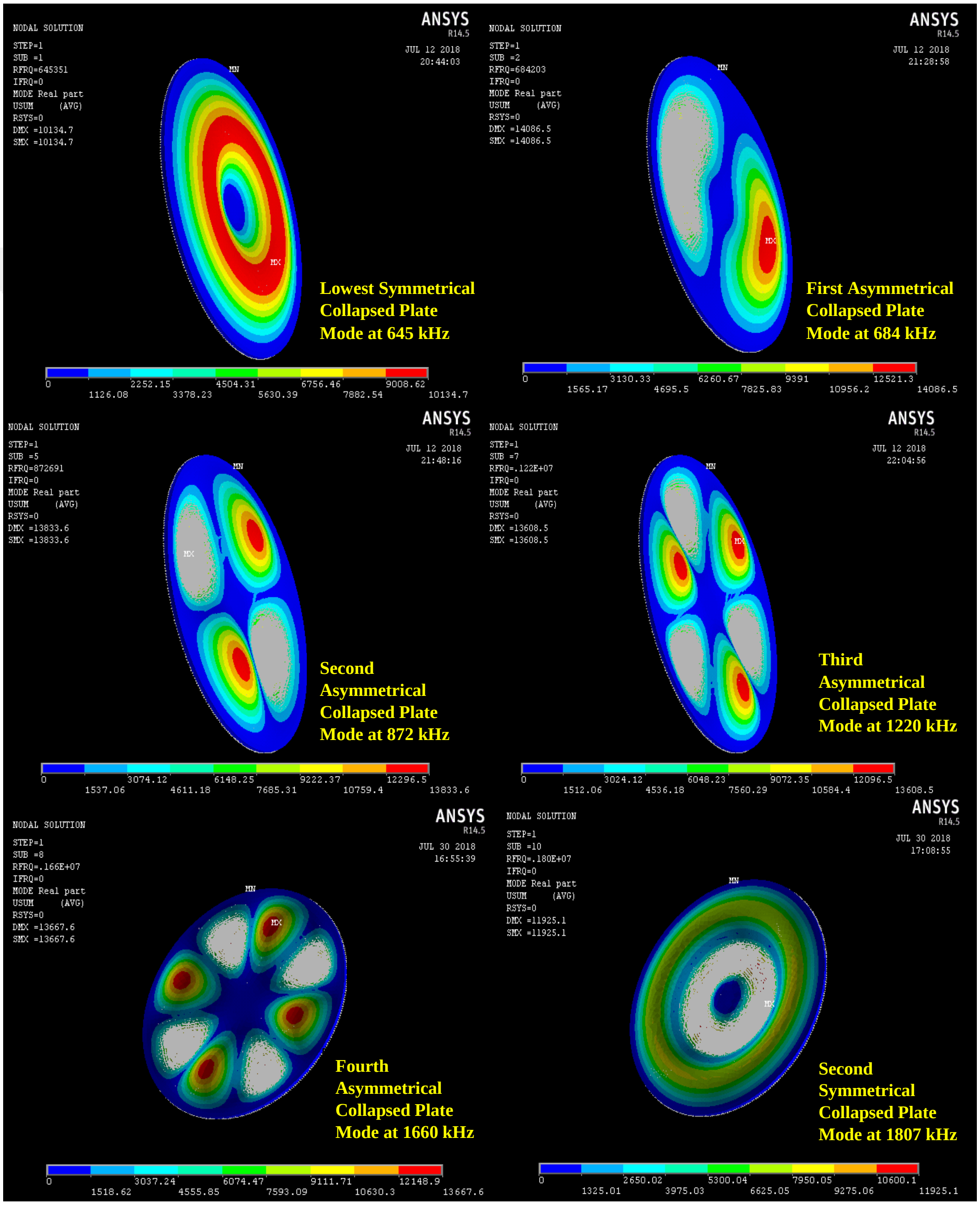

Figure 4.2: Collapsed CMUT plate modes obtained in FEM modal analysis.

We measure additional parasitic capacitance, C_p for both cells from the susceptance baseline as 0.98 times C_0. The insulation dielectric loss is modelled by G_i of (2.27) with loss tangent of silicon oxide, ($\tan\delta = 0.001$). In the model this dielectric loss can also be approximated by R_p in parallel with C_p. R_p manifests itself in conductance baseline at high frequencies. Both R_p and C_p are additional lumped elements and constitute electrical loss in the model.

At normalized gap height of 0.79, C_p of 0.98 times the clamped CMUT capacitance, C_0 effects the sensitivity multiplier term, h_1 of (2.35) by 3.1 dB in the critical biasing range where maximum open-circuit sensitivity is achieved. However, h_2 of (2.41) is not effected by the electrical losses, C_p and R_p. To measure the off-resonance SCRC of collapsed CMUT cells we employ a transimpedance amplifier with a capacitance feedback (similar to one described in [27]).

For CMUT-I, to match the measured resonance, we set $t_m = 15.4$ μm and $a = 492$ μm. The peak conductance is adjusted by setting $t_{ge} = 1.53$ μm which does not result in a significant shift in the resonance frequency. It must be noted that these physical dimensional parameters of CMUT may not reflect the actual CMUT dimensions but by considering such tolerances in the measured dimensions of Table I we can match the simulated admittance with the measured. These tolerances in physical dimensions effect CMUT operational parameters. For CMUT-I, F_b/F_g and t_g/t_{ge} are changed to 1.18, and 0.82, respectively. For CMUT-II same admittance characterizations were performed and we obtain $t_m = 15.51$ μm and $a = 490$ μm, plate thickness and radius respectively. The effective gap height, t_{ge} is set to 1.73μm. For CMUT-II, F_b/F_g and t_g/t_{ge} are changed to 1.00, and 0.75, respectively.

SCRC performance of fabricated cells is then re-derived at low frequencies with the modified CMUT operational parameters and the backing loss impedance. We

Table 4.2: Collapsed Plate Modes obtained in FEM Simulations.

First Symmetrical Mode	$645\,kHz$
First Asymmetrical Mode	$684\,kHz$
Second Asymmetrical Mode	$872\,kHz$
Third Asymmetrical Mode	$1220\,kHz$
Fourth Asymmetrical Mode	$1660\,kHz$
Second Symmetrical Mode	$1807\,kHz$

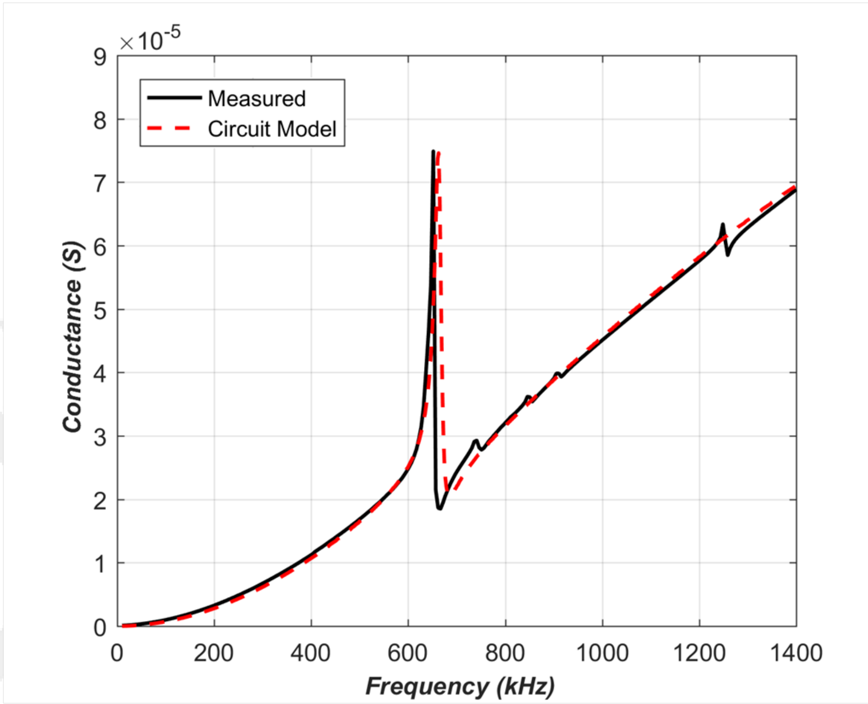

(a) **CMUT-I**

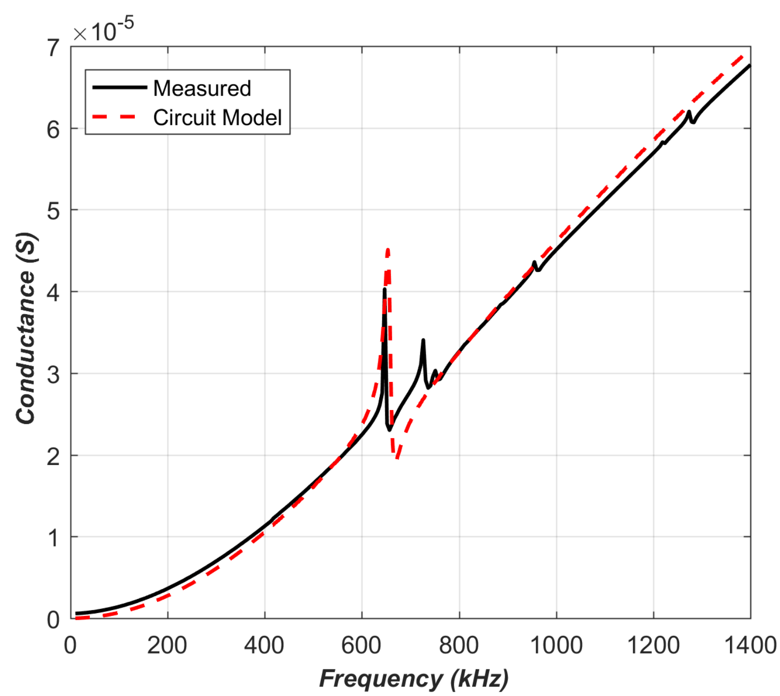

(b) **CMUT-II**

Figure 4.3: Measured and simulated conductance of fabricated CMUT cells.

characterize the model performance against the measured CMUT performance at off-resonance using the pitch-catch setup of Fig. 4.4.

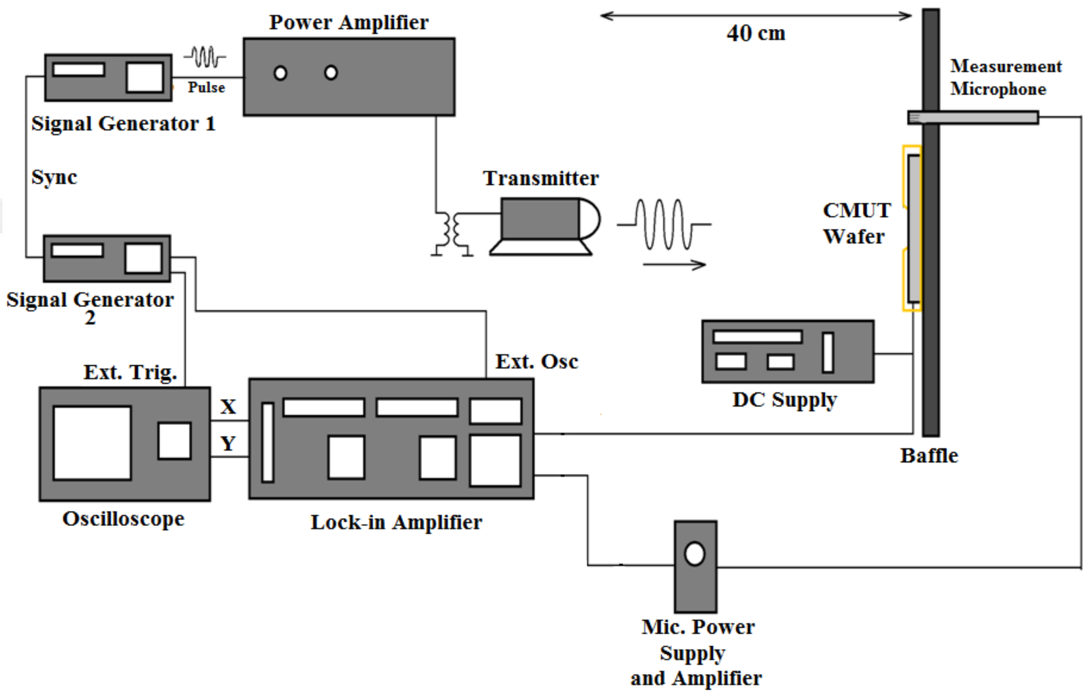

Figure 4.4: Time domain pulse measurement setup with lock-in amplifier and oscilloscope.

4.1.1 Receive Sensitivity Performance Measurements

SCRC sensitivity of CMUT-I and CMUT-II is measured at various low (off-resonance) frequencies using the setup shown in Fig. 4.4. First, the CMUT wafer is covered with a metal shield to reduce the coupling. A low noise OPAMP (MAX4475)[6] in a shield is placed right next to CMUT with $R_f = 1$ GΩ and $C_f = 1$ pF as its parallel feedback impedance. CMUT is connected directly to the inverting input while the non-inverting input of the OPAMP is connected to the ground. CMUT bias voltage is applied to the bottom electrode.
The output voltage of amplifier, $(i_{sc}/\omega C_f)$ is recorded with varying bias at each

[6]Maxim Integrated 160 Rio Robles, San Jose, CA, www.maximintegrated.com

frequency. The small-signal model of Fig. 2.4 is simulated in a circuit simulator[7] using the employed OPAMP at off-resonance, to include the pre-amplifier gain in SCRC as shown in Figures 4.5 to 4.11.

4.1.2 Pulse Measurements

Receiver CMUT is mounted 40 cm away on a planar wooden hardboard baffle, and is insonified by a wideband airborne transmitter[8] which is driven by a signal generator with a of 3 V_p pulse of 1 ms duration (100 cycles at 100 kHz). A gain of 75 is provided by a power amplifier[9]. Pulse repetition rate is kept 200 ms, to avoid any interference due to reflections or incoming transmitting pulse (See Fig. 4.5a).

A lock-in amplifier (Stanford Research Systems, SRS 830) with a set time constant of 100 μs and filter roll off of 12 dB/octave is employed to measure the amplitudes of receive signal envelopes on an oscilloscope. The incident acoustic pressure is first measured by a calibrated pressure microphone (pressure-field microphone, B&K 4138) mounted on a preamplifier (B&K 2633) using an adaptor (B&K UA 160). The microphone is polarized by a power supply (B&K Type 2807). The sensitivity of the microphone sub system is -66.9 dB V/Pa (or 0.452 mV/Pa). The microphone output voltage is converted into pressure using its calibration data and referred to the second axis at the right of Fig. 4.5a.

At the same distance of 40 cm, we measure the baffle pressure of 0.12 Pa. This reference pressure is used to normalize the received CMUT acoustic envelopes of Fig. 4.5b for varying DC bias. Measured sensitivity of fabricated CMUT cell is then compared with the model prediction at 100kHz (Fig. 4.5c). We repeat the pulse measurements at alternate off-resonance frequencies of 50, 90 and 110kHz with the same pulse excitation duration of 1 ms (no. of cycles are adjusted at each measurement frequency to maintain same pulse duration). The variation of of measured CMUT sensitivity against model is shown in Fig. 4.5 to 4.11.

[7] Advanced Design Systems, Keysight Technologies, Santa Rosa, CA.
[8] Series 600 Instrument Grade, Ultrasonic Transmitter, SensComp Inc. Livonia, USA
[9] Krohn-Hite 7500, Krohn-Hite Corporation, Brockton, MA

Separation of 40 cm between the ultrasound projector and receiver CMUT is maintained at each ultrasound frequency to provide more than the range required by 1 ms pulse time travel. Received acoustic envelope amplitude is obtained from the in phase (X) and quadrature (Y) outputs of the lock in amplifier. CMUT receive signal amplitude variation with bias is shown at each frequency (Fig. 4.5 to 4.11). We record multiple receive envelopes at each bias with a variance of less than 2 dB. Averaged envelopes are shown in this thesis. Average SNR of these measurements for varying bias is about 21 dB. We report absolute pressure measurements in air which are affected by the measurement environment differently at different frequencies.

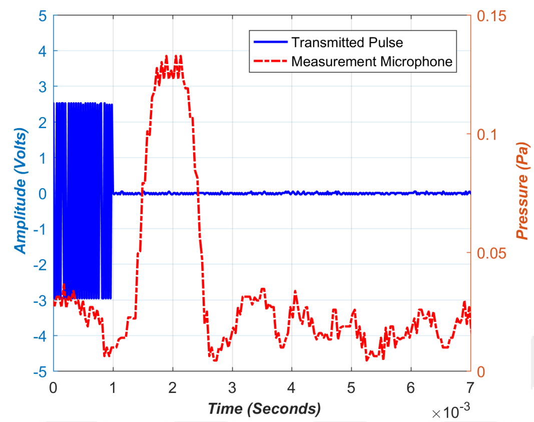

(a) Transmitted Pulse and Measurement Microphone Recorded Pressure

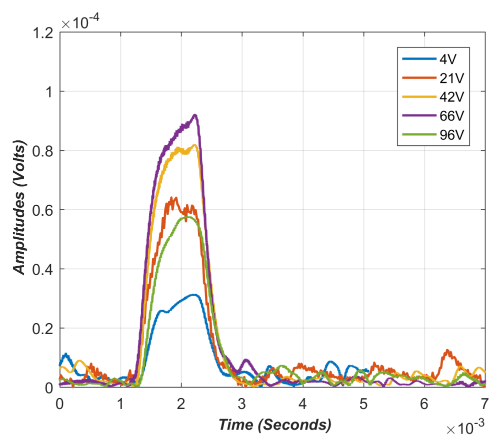

(b) Received Signal Envelopes

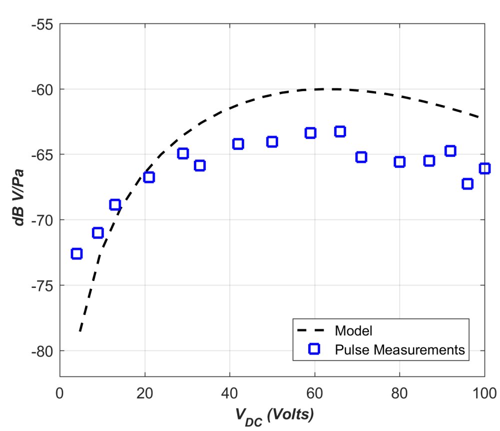

(c) Normalized SCRC Measurements

Figure 4.5: CMUT-I Pulse Measurements at 50kHz (a) transmitted pulse and measurement microphone recorded pressure (b) received signal envelopes for varying DC bias (c) squares in the figure shows the measured sensitivity at 50kHz.

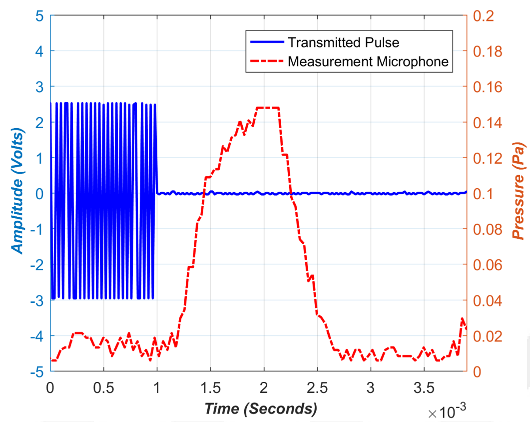

(a) Transmitted Pulse and Measurement Microphone Recorded Pressure

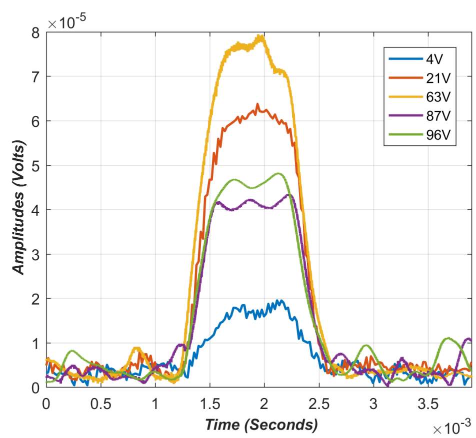

(b) Received Signal Envelopes

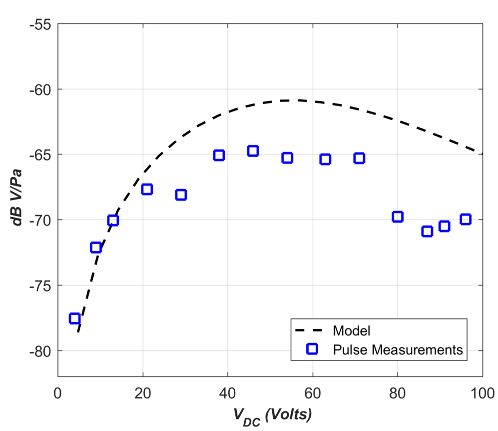

(c) Normalized SCRC Measurements

Figure 4.6: CMUT-I Pulse Measurements at 90kHz (a) transmitted pulse and measurement microphone recorded pressure (b) received signal envelopes for varying DC bias (c) squares in the figure shows the measured sensitivity at 90kHz.

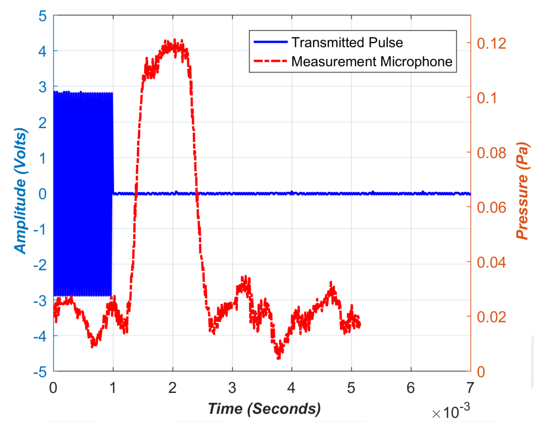

(a) Transmitted Pulse and Measurement Microphone Recorded Pressure

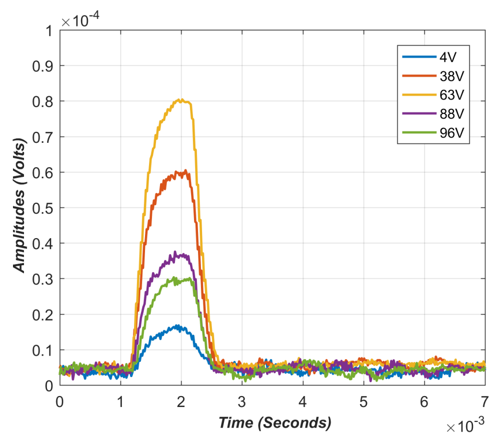

(b) Received Signal Envelopes

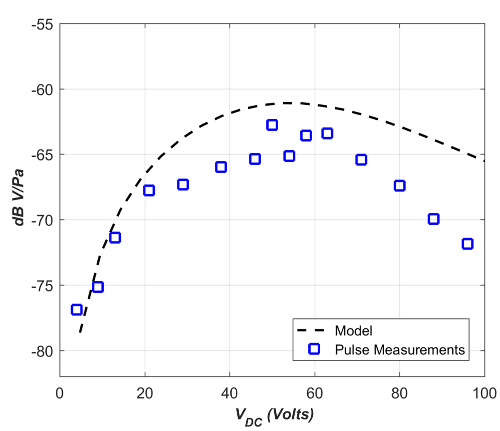

(c) Normalized SCRC Measurements

Figure 4.7: CMUT-I Pulse Measurements at 100kHz (a) transmitted pulse and measurement microphone recorded pressure (b) received signal envelopes for varying DC bias (c) squares in the figure shows the measured sensitivity at 100kHz.

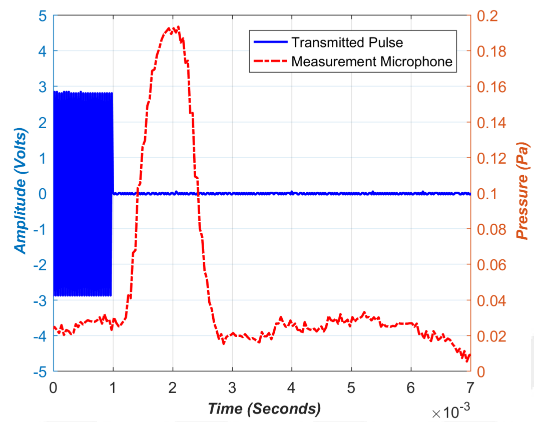

(a) Transmitted Pulse and Measurement Microphone Recorded Pressure

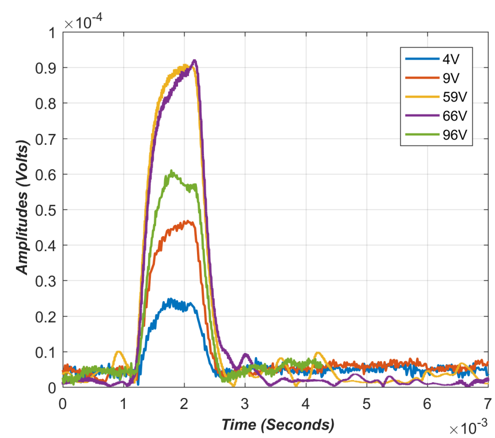

(b) Received Signal Envelopes

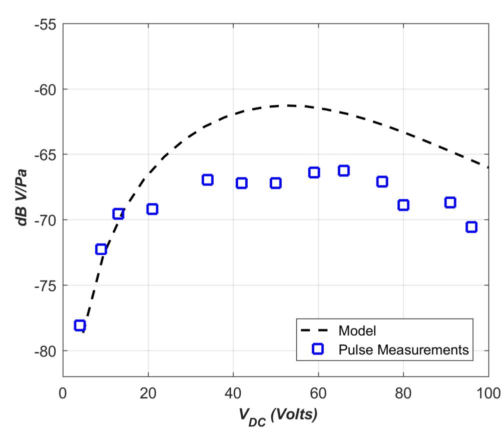

(c) Normalized SCRC Measurements

Figure 4.8: CMUT-I Pulse Measurements at 110kHz (a) transmitted pulse and measurement microphone recorded pressure (b) received signal envelopes for varying DC bias (c) squares in the figure shows the measured sensitivity at 110kHz.

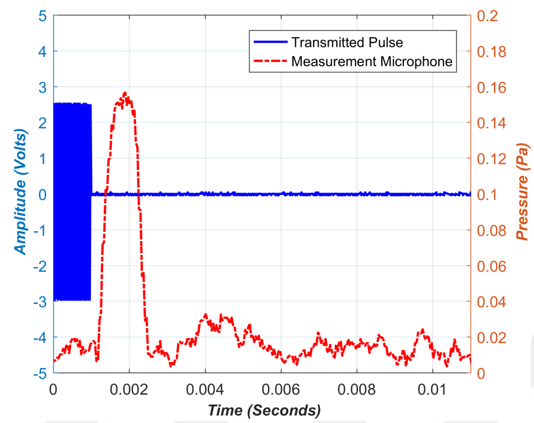

(a) Transmitted Pulse and Measurement Microphone Recorded Pressure

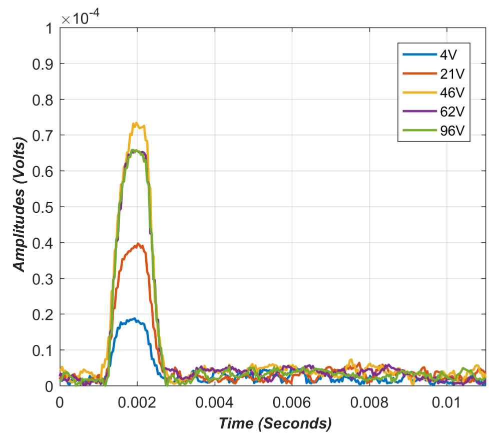

(b) Received Signal Envelopes

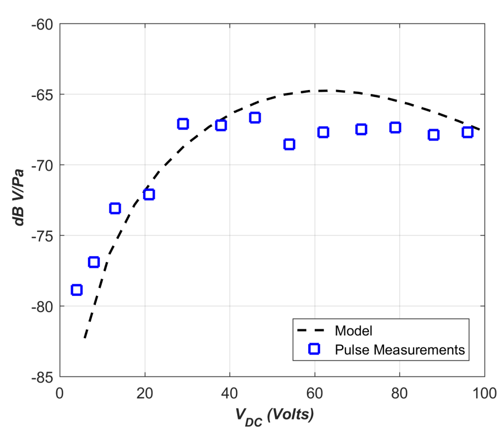

(c) Normalized SCRC Measurements

Figure 4.9: CMUT-II Pulse Measurements at 50kHz (a) transmitted pulse and measurement microphone recorded pressure (b) received signal envelopes for varying DC bias (c) squares in the figure shows the measured sensitivity at 50kHz.

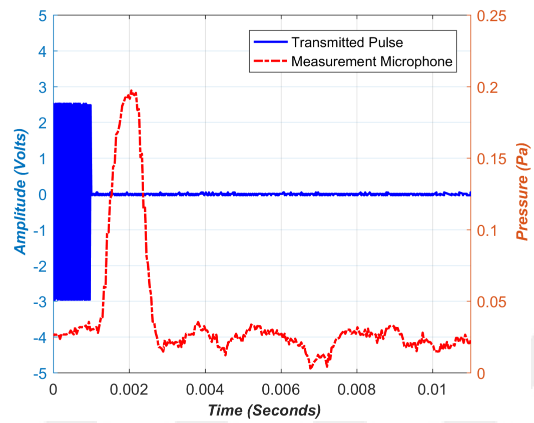

(a) Transmitted Pulse and Measurement Microphone Recorded Pressure

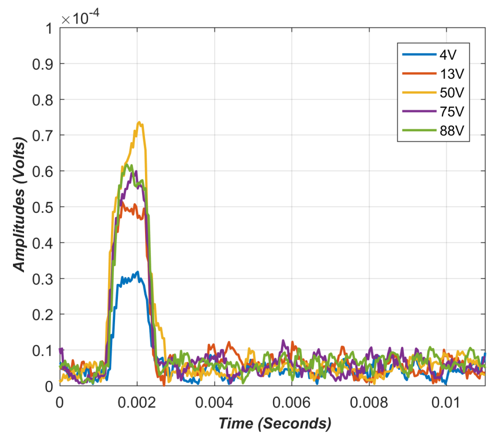

(b) Received Signal Envelopes

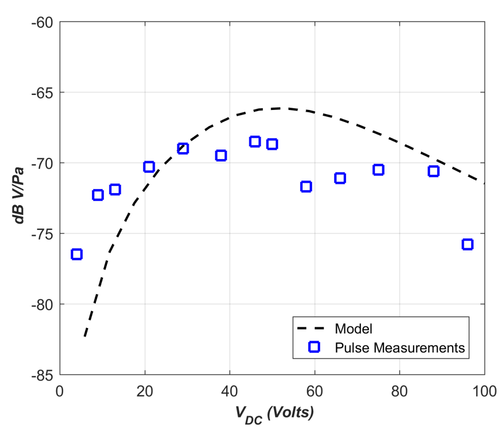

(c) Normalized SCRC Measurements

Figure 4.10: CMUT-II Pulse Measurements at 90kHz (a) transmitted pulse and measurement microphone recorded pressure (b) received signal envelopes for varying DC bias (c) squares in the figure shows the measured sensitivity at 90kHz.

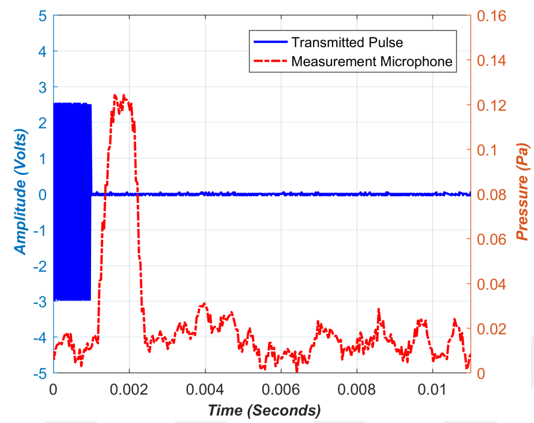

(a) Transmitted Pulse and Measurement Microphone Recorded Pressure

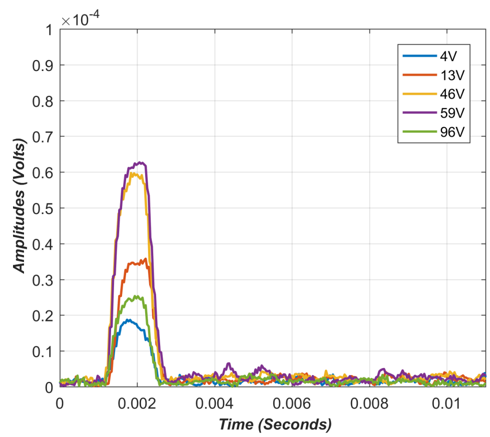

(b) Received Signal Envelopes

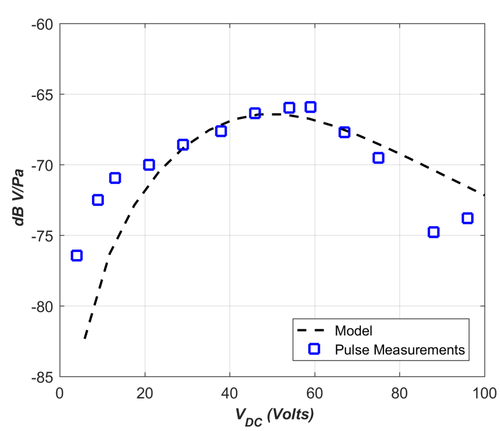

(c) Normalized SCRC Measurements

Figure 4.11: CMUT-II Pulse Measurements at 100kHz (a) transmitted pulse and measurement microphone recorded pressure (b) received signal envelopes for varying DC bias (c) squares in the figure shows the measured sensitivity at 100kHz.

4.2 Discussion

Measured absolute receive sensitivity of collapsed CMUT receivers is in very good agreement with what is predicted by our small signal model. The critical biasing region predicted by the model of fabricated CMUT is characterized within 3 dB on average at various off-resonance frequencies. The measured data points are averaged at the same bias with maximum variance less than 2 dB. The difference between the model predictions and measurements are likely due to the diffraction effects due to the large aperture size of the projector and the separation between the measurement microphone and the CMUT cells on the hardboard baffle. The separation between the receivers cannot be decreased due to the size of the glass wafer. We report absolute pressure measurements in air in this thesis which are affected by the measurement environment differently at different frequencies.

Also, based on admittance measurements we modified the equivalent circuit model. These modifications are made considering the tolerances in the physical CMUT dimensions, however fitting the simulated admittance over measuremnts may not reflect the actual CMUT geometry but is a mere representation of a combination of CMUT dimensions with assumed material properties that best explain the measurements. However this solution is not unique. Residual stress in the plate could be another factor however, we do not consider the effect of residual stress separately. Because it modifies the Youngs modulus additively and it is usually few orders of magnitude low.

As a part of the modification, loss mechanisms are also introduced in both the electrical and the mechanical side. Unlike conventional CMUT, we observed that some part of the incoming ultrasound energy is lost in the backing in collapsed-mode of operation in form of spherical waves propagating into the solid half space as in [26]. This backing loss is modelled by the loss resistance and a series backing compliance that reproduces the measured baseline in conductance but at the same time degrades the receive performance of a collapsed CMUT transducer.

Chapter 5

Conclusions

In this work, we derive and use a linear circuit model to optimize collapsed CMUT receiver performance at low frequencies compared to resonance. We identified that irrespective of CMUT geometry, in collapsed mode of operation there always exists a maximum sensitivity region where if the transducer is biased, a stable and maximum receive signal is produced. We demonstrated that fabricated collapsed CMUT cell maximum receive sensitivity can be very accurately characterized by our linear small signal model.

We first measure and characterize the admittance of fabricated cells. We measured fundamental resonance of fabricated cells at 650 kHz with a quality factor of 68. The small resonance peaks at high frequencies in measured conductance of collapsed CMUT cells are lowest order plate asymmetrical modes above the fundamental symmetrical plate mode of 645kHz. The baseline of measured conductance is reproduced by adding the radiation resistance of spherical waves propogating in the backing material. We also found that for lower measured quality factor of 68, collapsed CMUT exhibits significant friction loss in plate material compared to an un-collapsed CMUT.

We were able to characterize the critical biasing region of fabricated collapsed CMUT cells by varying the DC bias at low frequencies. Collapsed CMUT performance is measured and characetrized for various off-resonance ultrasound frequencies. Besides an optimized receive performance, collapsed CMUTs produce a stable sensitivity compared to an un-collapsed mode of CMUT operation where the plate is biased at 80-90% of collapse voltage to favor improved coupling conditions.

We measured two fabricated CMUT cells at low frequencies which are collapsed initially under the effect of ambient force only (without any bias). We experimentally characterized the SCRC performance using a transimpedance amplifier. We measured and characterized an off-resonance performance of -60 dB V/Pa for CMUT-I at various ultrasound frequencies when they are biased between 50 to 65 Volts. For CMUT-II we measure -65 dB V/Pa over a biasing range of 40 to 60 Volts. For given operating conditions of collapsed CMUTs, the performance design curves dictate the maxima performance region where the cell should be biased, if it is biased beyond this region the spring becomes hard and impairs the performance. Moreover, the backing loss lowers the receive SNR of CMUT receivers as part of the receive ultrasound is absorbed in the backing.

At low frequencies the radiation resistance is small and can be ignored making the immersion medium less important for optimizing the performance of a collapsed cell. The series loss which accounts for collapsed plate friction, is also overwhelmed by series plate compliance at low frequencies and hence does not effect the off-resonance performance of a collapsed CMUT. We measured C_p as 0.98 times CMUT clamped CMUT capacitance, C_0 from the susceptance baseline. This additional parasitic capacitance effects the open circuit voltage of CMUT by 3.1 dB in the critical biasing region where maxima is acheived. To eliminate this electrical loss due to C_p we used a transimpedance amplifier that virtually ground C_p and does not let it impair the preamplifier output.

Bibliography

[1] O. Oralkan, A. S. Ergun, J. A. Johnson, M. Karaman, U. Demirci, K. Kaviani, T. H. Lee, and B. T. Khuri-Yakub, "Capacitive micromachined ultrasonic transducers: Next-generation arrays for acoustic imaging?," *IEEE Transactions on Ultrasonics, Ferroelectrics, and Frequency Control*, vol. 49, no. 11, pp. 1596–1610, 2002.

[2] D. M. Mills and L. S. Smith, "Real-time in-vivo imaging with capacitive micromachined ultrasound transducer (CMUT) linear arrays," in *Ultrasonics, 2003 IEEE Symposium*, vol. 1, pp. 568–571, IEEE, 2003.

[3] D. M. Mills, "Medical imaging with capacitive micromachined ultrasound transducer (CMUT) arrays," in *Ultrasonics Symposium, 2004 IEEE*, vol. 1, pp. 384–390, IEEE, 2004.

[4] C. H. Cheng, E. M. Chow, X. Jin, S. Ergun, and B. T. Khuri-Yakub, "An efficient electrical addressing method using through-wafer vias for two-dimensional ultrasonic arrays," in *Ultrasonics Symposium, 2000 IEEE*, vol. 2, pp. 1179–1182, IEEE, 2000.

[5] J. F. Kuhmann, M. Heschel, S. Bouwstra, F. Baleras, and C. Massit, "Through wafer interconnects and flip-chip bonding: A toolbox for advanced hybrid technologies for MEMS," in *13th European Conference on Solid-State Transducers*, pp. 265–72, 1999.

[6] M. Pekař, W. U. Dittmer, N. Mihajlović, G. van Soest, and N. de Jong, "Frequency tuning of collapse-mode capacitive micromachined ultrasonic transducer," *Ultrasonics*, vol. 74, pp. 144–152, 2017.

[7] B. Bayram, E. Hæggstrom, G. G. Yaralioglu, and B. T. Khuri-Yakub, "A new regime for operating capacitive micromachined ultrasonic transducers," *IEEE Transactions on Ultrasonics, Ferroelectrics, and Frequency Control*, vol. 50, no. 9, pp. 1184–1190, 2003.

[8] O. Oralkan, B. Bayram, G. G. Yaralioglu, A. S. Ergun, M. Kupnik, D. T. Yeh, I. O. Wygant, and B. T. Khuri-Yakub, "Experimental characterization of collapse-mode CMUT operation," *IEEE Transactions on Ultrasonics, Ferroelectrics, and Frequency Control*, vol. 53, no. 8, pp. 1513–1523, 2006.

[9] S. Olcum, F. Y. Yamaner, A. Bozkurt, H. Köymen, and A. Atalar, "Deep-collapse operation of capacitive micromachined ultrasonic transducers," *IEEE Transactions on Ultrasonics, Ferroelectrics, and Frequency Control*, vol. 58, no. 11, pp. 2475–2483, 2011.

[10] K. K. Park, O. Oralkan, and B. T. Khuri-Yakub, "A comparison between conventional and collapse-mode capacitive micromachined ultrasonic transducers in 10-MHz 1-D arrays," *IEEE Transactions on Ultrasonics, Ferroelectrics, and Frequency Control*, vol. 60, no. 6, pp. 1245–1255, 2013.

[11] Y. Huang, E. Haeggstrom, B. Bayram, Z. Zhuang, A. Ergun, C. Cheng, and B. Khuri-Yakub, "Collapsed regime operation of capacitive micromachined ultrasonic transducers based on wafer-bonding technique," in *Ultrasonics, 2003 IEEE Symposium on*, vol. 2, pp. 1161–1164, IEEE, 2003.

[12] E. Aydogdu, A. Ozgurluk, A. Atalar, and H. Koymen, "Parametric nonlinear lumped element model for circular CMUTs in collapsed mode," *IEEE Transactions on Ultrasonics, Ferroelectrics, and Frequency Control*, vol. 61, no. 1, pp. 173–181, 2014.

[13] E. Aydogdu, A. Ozgurluk, H. K. Oguz, A. Atalar, and H. Koymen, "Lumped element model of single CMUT in collapsed mode," in *Ultrasonics Symposium (IUS), 2013 IEEE International*, pp. 283–286, IEEE, 2013.

[14] E. Aydoğdu, *Lumped element modeling of circular CMUT in collapsed mode.* PhD thesis, Bilkent University, 2014.

[15] H. Koymen, A. Atalar, E. Aydogdu, C. Kocabas, H. K. Oguz, S. Olcum, A. Ozgurluk, and A. Unlugedik, "An improved lumped element nonlinear circuit model for a circular CMUT cell," *IEEE Transactions on Ultrasonics, Ferroelectrics, and Frequency Control*, vol. 59, no. 8, 2012.

[16] A. Ozgurluk, A. Atalar, H. Koymen, and S. Olcum, "Radiation impedance of collapsed capacitive micromachined ultrasonic transducers," *IEEE Transactions on Ultrasonics, Ferroelectrics, and Frequency Control*, vol. 59, no. 6, pp. 1301–1308, 2012.

[17] A. Unlugedik, A. S. Tasdelen, A. Atalar, and H. Koymen, "Designing transmitting CMUT cells for airborne applications," *IEEE Transactions on Ultrasonics, Ferroelectrics, and Frequency Control*, vol. 61, no. 11, pp. 1899–1910, 2014.

[18] A. S. Savoia, B. Mauti, and G. Caliano, "Accurate evaluation of the electromechanical and parasitic parameters of CMUTs through electrical impedance characterization," in *Ultrasonics Symposium (IUS), 2017 IEEE International*, pp. 1–4, IEEE, 2017.

[19] C. Meynier, D. Certon, F. Teston, N. Felix, and G. Ferin, "P4m-5 accurate assessment of CMUT devices through precise electrical impedance measurement in air," in *Ultrasonics Symposium, 2007. IEEE*, pp. 2139–2142, IEEE, 2007.

[20] H. Köymen, A. Atalar, and A. S. Taşdelen, "Bilateral CMUT cells and arrays: Equivalent circuits, diffraction constants, and substrate impedance," *IEEE Transactions on Ultrasonics, Ferroelectrics, and Frequency Control*, vol. 64, no. 2, pp. 414–423, 2017.

[21] H. Köymen, A. Atalar, and H. K. Oğuz, "Designing circular CMUT cells using CMUT biasing chart," in *Ultrasonics Symposium (IUS), 2012 IEEE International*, pp. 975–978, IEEE, 2012.

[22] A. S. Ergun, G. G. Yaralioglu, and B. T. Khuri-Yakub, "Capacitive micromachined ultrasonic transducers: Theory and technology," *Journal of Aerospace Engineering*, vol. 16, no. 2, pp. 76–84, 2003.

[23] M. Kupnik, I. O. Wygant, and B. T. Khuri-Yakub, "Finite element analysis of stress stiffening effects in cmuts," in *Ultrasonics Symposium, 2008. IUS 2008. IEEE*, pp. 487–490, IEEE, 2008.

[24] A. Unlugedik, A. Atalar, and H. Koymen, "Designing an efficient wide bandwidth single cell cmut for airborne applications using nonlinear effects," in *Ultrasonics Symposium (IUS), 2013 IEEE International*, pp. 1416–1419, IEEE, 2013.

[25] M. Bellaredj, G. Bourbon, V. Walter, P. Le Moal, and M. Berthillier, "Anodic bonding using SOI wafer for fabrication of capacitive micromachined ultrasonic transducers," *Journal of Micromechanics and Microengineering*, vol. 24, no. 2, p. 025009, 2014.

[26] F. Blake Jr, "Spherical wave propagation in solid media," *The Journal of the Acoustical Society of America*, vol. 24, no. 2, pp. 211–215, 1952.

[27] H. Köymen, A. Atalar, S. Güler, I. Köymen, A. S. Taşdelen, and A. Ünlügedik, "Unbiased charged circular CMUT microphone: Lumped-element modeling and performance," *IEEE transactions on ultrasonics, ferroelectrics, and frequency control*, vol. 65, no. 1, pp. 60–71, 2018.

Appendix A

Collapsed-mode CMUT Capacitance and Compliance Polynomials

$g_c(.)$ in (2.10) is a polynomial in X_R/t_{ge} corresponding to the CMUT nonlinear capacitance

$$g_c\left(\frac{X_R}{t_{ge}}\right) = \sum_{i=0}^{3} n_i \left(\frac{X_R}{t_{ge}}\right)^i \tag{A.1}$$

For a given CMUT design first the operational parameters are determined from its physical dimensional parameters. For the obtained fixed normalized static pressure, P_b/P_g , and gap height, t_g/t_{ge}, (2.2) is solved by varying V_{DC}/V_r. This yields values for the collapsed bending profile, $\overline{x}(\overline{r})$. Corresponding nonlinear CMUT capacitance C for each given deflection profile $\overline{x}(\overline{r})$ is obtained from (A.2) as:

$$C = C_0 \int_0^1 \frac{2\overline{r}}{1-\overline{x}(\overline{r})} d\overline{r} \tag{A.2}$$

For each collapsed profile $\overline{x}(\overline{r})$, (A.2) is solved numerically in the MATLAB routine of [14] and corresponding values for normalized capacitance, C/C_0 are obtained. A third degree curve fitting to C/C_0 against X_R/t_{ge} yields polynomial coefficients n_i of (A.1).

Fig. A.1 plots $g_c(.)$ as normalized CMUT electrical capaciatance of (2.10), C_{0dc}/C_0 versus X_R/t_{ge} for varying normalized gap heights, t_g/t_{ge} and normalized force, F_b/F_g of 1. For large t_g/t_{ge} values collapsed CMUT capacitance is higher owing to thin insulation layer gap between the electrodes. As V_{DC} increases, plate contact area becomes large resulting in a higher capacitance.

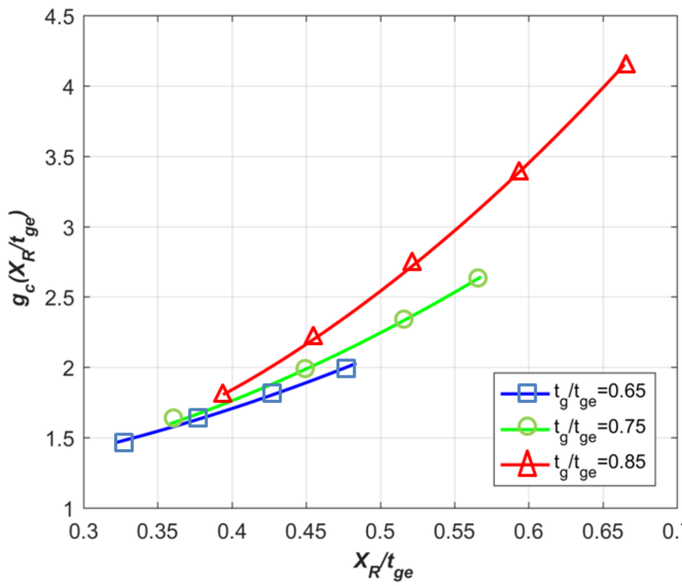

Figure A.1: CMUT capacitance polynomial, $g_c\left(\frac{X_R}{t_{ge}}\right)$ as a function of X_R/t_{ge} for varying normalized gap heights, t_g/t_{ge} and normalized force, F_b/F_g of 1.

Compliance in collapsed mode of operation is a nonlinear function of normalized *rms* plate displacement X_R/t_{ge} and decreases with increasing contact of plate on the substrate. We define C_{Rm} as the ratio of X_R to total *rms* force on the membrane (including both electrical and ambient force)

$$C_{Rm} = \frac{X_R}{F_R + F_{Rb}} \tag{A.3}$$

where F_R is the nonlinear electrical force of (2.12) and F_{Rb} is the *rms* static force due to ambient pressure P_b. Eq.(A.3) can be expressed in its normalized form as:

$$\frac{C_{Rm}}{C_{Rm0}} = \frac{\sqrt{5}(X_R/t_{ge})}{\frac{2\sqrt{5}}{15}\left(\frac{V_{DC}}{V_r}\right)^2 \frac{dC}{d\overline{X}_R} + \frac{P_b}{P_g}} \tag{A.4}$$

With C/C_0 data in hand, $dC/d\overline{X}_R$ is obtained from the first derivative of (A.2) numerically for any given P_b/P_g , and t_g/t_{ge} . A fourth degree curve fitting to the normalized compliance curve C_{Rm}/C_{Rm0} yields polynomial coefficients m_i for $h_c(.)$ of (2.21)

$$h_c\left(\frac{X_R}{t_{ge}}\right) = \sum_{i=0}^{4} m_i \left(\frac{X_R}{t_{ge}}\right)^i \tag{A.5}$$

For any arbitrary CMUT operating conditions once $g_c(.)$ and $h_c(.)$ polynomials are obtained, the sensitivity multiplier h_2 of the collapsed CMUT can be calculated from (2.41). SCRC performance can then be readily obtained from (2.40) for given material and physical dimensional parameters of CMUT. Table II contains the polynomial coefficients obtained for CMUT capacitance and compliance for normalized static pressure, P_b/P_g of 1.29 and normalized gap height, t_g/t_{ge} of 0.79.

Table A.1: Polynomial Coefficients for P_b/P_g of 1.29 and t_g/t_{ge} of 0.79.

n_i	n_0	n_1	n_2	n_3	
	0.9985	-0.7316	6.5870	0.3577	
m_i	m_0	m_1	m_2	m_3	m_4
	6.735	-22.330	8.3695	36.1269	-31.9043

Appendix B

Implementation of Small Signal Model in ADS

We realize our linear circuit model in Advanced Design Systems, (ADS, Keysight Technologies, Santa Rosa, CA) which is a suitable circuit design enviroment allowing the user to define nonlinear parametrical equations both in time and frequency domains. The expressions for model capacitance, compliance and their derivates are defined as polynomials in X_R/t_{ge}. Fig. B.1 show these expressions as ADS variables. These variables represent the lumped circuit elements of our model in Fig. B.2 (polynomial expressions for P_b/P_g of 1.29 and t_g/t_{ge} of 0.79 as in Table A.1 is only shown here).

The static operating point of the circuit is defined as normalized *rms* profile, X_R/t_{ge}, this is first evaluated numerically from Timoshenko's equations of (2.2) for any given operating conditions. CMUT operating conditions like P_b/P_g and t_g/t_{ge} are evaluated in ADS for the given physical dimensions and plate material properties. Once the normalized pressure and gap heights are fixed then if bias is changed the corresponding X_R/t_{ge} is re-evaluated and lumped elements are redefined automatically in the model for new X_R/t_{ge}. Once the lumped elements of the model are defined, a linear AC analysis produces circuit output paramaters like resonance, its quality factor and its performance throughout the frequency sweep.

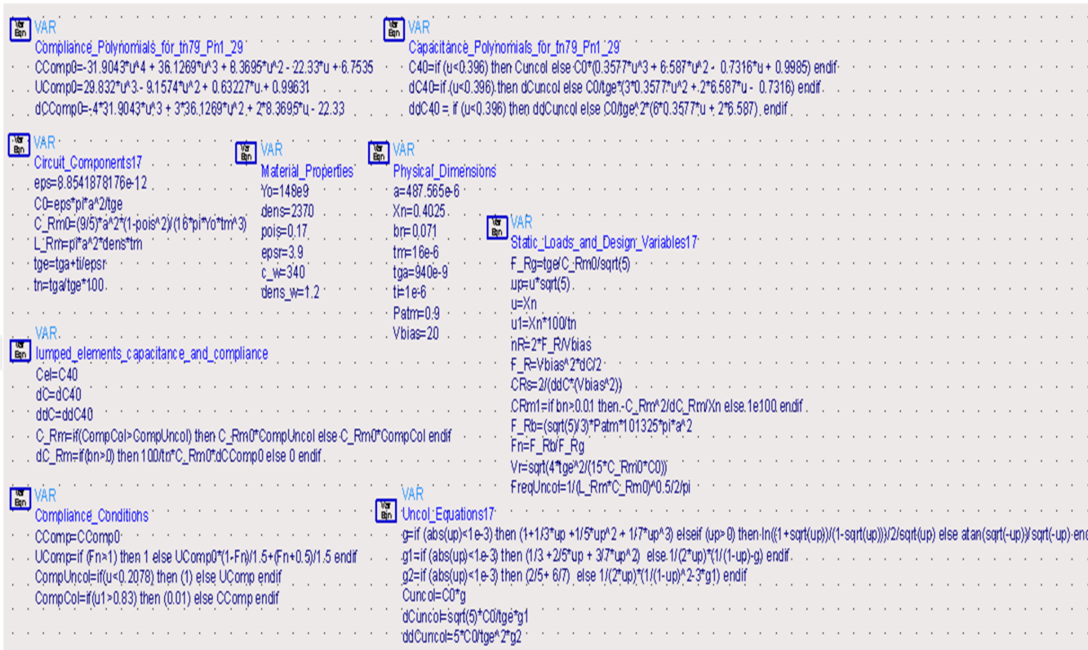

Figure B.1: ADS variables for model capacitance and compliance and their derivatives for P_b/P_g of 1.29 and t_g/t_{ge} of 0.79.

User can add external circuit elements like series loss resistor, parasitic capaciatance and die-electric loss resistance as shown in Fig. 2.4 to for a complete assesement of electrodynamic behaviour of transducer. These external lumped circuit elements can be obtained from admittance measurement data as explained in Chapter 2.

On the electrical side of the circuit "Cell" represents C_{0dc} which has a polynomial expression defined in Fig. B.1. Linear rransduction force, f_r is handeled by a transformer with turns ratio "nR" and the spring softening capacitance, C_{Rs}. Negative sign infront of spring softening capacitor represents the opposing direction of electrical force compared to plate restoring force. Next two capacitances "CRm1" and "C Rm" represent the DC and AC plate compliances. Series combination of these two capaciatnces is refered as C_{Rms} in Chapter 2. The inertial force of the plate is represented with an inductor, inductance of which is equal to the mass of the plate in rms model. The expressions for the model capacitances

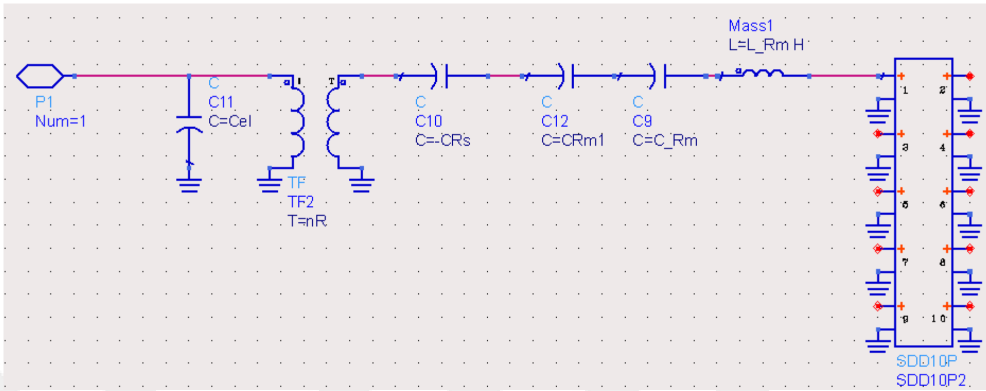

Figure B.2: Small signal model for collapsed CMUT with its self radiation impedance only.

and inductor is defined in "Static load and design" variable and "Circuit Component" variable of Fig. B.1.

The acoustic port is finally terminated in the self radiation impedance of the cell. In single CMUT simulations only the first port of SDD block containing the self radiation impedance of cell is used. The other mechanical ports of SDD block are used in array simulations with multiple cells. The same block can be used to introduce the mutual impedance between neighboring cells. The self radiation impedance is defined through lookup tables as functions of contact radius and ka.

Each of the "access data" commands introduce the impedance as a function of ka at a fixed value of contact radius, b. This command reads the impedance from the lookup table in the related ".ds"" document, and interpolates in frequency domain. There are nine data readers for b= 0, 0.5, 0.1, 0.15, 0.2, 0.3, 0.4, 0.5 and 0.6. In the SDD block, interpolation is performed between impedance functions of discrete b.

Appendix C

FEM Modal Analysis - Ansys APDL Code

FEM simulations shown in Fig. 4.2 are carried out in Ansys R14.5 (Ansys Inc., Canonsburg, PA). Modal analysis of the collapsed CMUT plate is done and the first symmetrical mode and asymmetrical modes below the second symmetrical mode are extracted.

```
finish
/clear, nostart
/prep7


!!!!!!!! PARAMETERS!!!!!!!!

pi = 4*ATAN(1)

!!!!!!!! ELEMENT TYPES !!!!!!!!
et,11,200,7
ET,1,SOLID186,
```

```
!!!!!!!! MATERIAL PROPERTIES !!!!!!!!
! Material properties for silicon
e_s = 148e9
dens_s = 2370
poiss_s  = 0.17

SIO2_eps = 3.7

mp, ex, 1, e_s ! Material 1 is silicon
mp, dens, 1, dens_s
mp, nuxy, 1, poiss_s

!!!!!!!! GEOMETRY !!!!!!!!

cmut_rad = 485e-6
cmut_thick = 15.42e-6
cmut_gap = 0.98e-6
cmut_ti = 1e-6

cmut_mesh_size =  cmut_thick
cmut_mesh_div = 40


! Transducer
CYLIND,cmut_rad,0,0,-cmut_thick,0,360


! Mesh the CMUT
! Divide the thickness of the CMUT
csys,0
lsel,s,loc,z,-cmut_thick
lesize,all,,,cmut_mesh_div
alls
```

```
csys,0
ASEL,S,LOC,Z,-cmut_thick
lsla,s
ksll,s
type,11
MSHAPE,0,2D
MSHKEY,0
*GET,A1, AREA,0,NUM,MIN
*GET,K1, KP,0,NUM,MIN
K2=KPNEXT(K1)
K3=KPNEXT(K2)
K4=KPNEXT(K3)
ESIZE,cmut_mesh_size
AMESH,ALL

vsla,s
cm,cmut_vol,volu

ESIZE,cmut_mesh_size
VATT,1,,1
VSWEEP,ALL
ACLEAR,ALL
alls

! TRANS126
csys,1
asel, s,loc, x, 0,cmut_rad
asel, r,loc, z, -cmut_thick
nsla, s, 1
cm,ELECT,node
csys,0
```

```
!************************************
! Place TRANS126 elements
EMTGEN, 'ELECT','MEMBRANE','GROUND', 'UZ',
-CMUT_GAP -CMUT_TI/SIO2_eps,
CMUT_TI/SIO2_eps, 1 ,8.854e-12
!************************************

D,ground,UX,0
D,ground,UY,0
D,ground,UZ,0
D,ground,VOLT,0
ALLS
nsel, s,,, ELECT
cp,1,VOLT,all      ! COUPLE TOP ELECTRODE
*get,NTOP,NODE,0,num,min    ! GET MASTER NODE ON TOP ELECTRODE
nsel,all

csys,0
asel,s,loc,z,-cmut_thick/2
asel,u,loc,x,cmut_rad/2
asel,u,loc,y,cmut_rad/2
nsla,s,1
D,all,UX,0
D,all,UY,0
D,all,UZ,0
alls

csys,1
asel, s,loc, x, 0,cmut_rad
asel, r,loc, z, 0
nsla, s, 1
cm,srf_nodes,node
alls
```

```
FINISH
/SOLU
ANTYPE,STATIC
PSTRES,ON
!NLGEOM, ON    ! Include Large deflections.
neqit,100
csys,1
asel, s,loc, x, 0,cmut_rad
asel, r,loc, z, 0
SFA, all, ,PRES, 101325 ! 101325 Pa = 1atm
ALLS
D, NTOP, VOLT, 20
cnvtol,u
!cnvtol,f
ALLS
SOLVE
!UPCOORD,1,ON
FINISH
/SOLU
ANTYPE,modal
MODOPT,UNSYM,40
MXPAND
PSTRES,on
allsel, all, all
SOLVE
FINISH
!*******
/post1
!SET,1,1
PLDISP,1
```